

RESPONSE TO EDITOR'S COMMENTS

Comments to the Author:

- I agree with the reviewer, and think that the last three sentences of the abstract are too speculative and misleading, please remove them: "However, the very large fraction of the emissions deposited on the Greenland Ice Sheet makes these fires very efficient climate forcers on a per unit emission basis. If the expected future warming of the Arctic produces more severe fires in Greenland, this could indeed cause albedo changes and thus contribute to accelerated melting of the Greenland Ice Sheet. The fires burning in 2017 may be a harbinger of such future events."

This is a local effect, and saying that they are very efficient climate forcers is misleading even if these fires become two orders of magnitude larger.

Maybe something along these lines is more appropriate:

However, the very large fraction of the emissions deposited on the Greenland Ice Sheet from these fires could contribute to accelerated melting of the Greenland Ice Sheet if these fires become several (1-2??) orders of magnitude larger under future climate.

RESPONSE: We agree and have corrected it as the Editor suggested.

Please address this issue in the conclusion too.

RESPONSE: Conclusions were corrected it as the Editor suggested.

- In section 4.1 please use "to evaluate" rather than "to validate".

RESPONSE: Corrected in the text and title of section 4.1 (see track changes).

- L938. There are two "on" please correct that.

RESPONSE: Corrected (see track changes on Conclusions section).

1 **Open fires in Greenland in summer 2017: transport,**
2 **deposition and radiative effects of BC, OC and BrC**
3 **emissions**

4

5 **Nikolaos Evangeliou^{1,*}, Arve Kylling¹, Sabine Eckhardt¹, Viktor Myroniuk²,**
6 **Kerstin Stebel¹, Ronan Paugam³, Sergiy Zibtsev², Andreas Stohl¹**

7

8 ¹Norwegian Institute for Air Research (NILU), Department of Atmospheric and Climate
9 Research (ATMOS), Kjeller, Norway.

10 ²National University of Life and Environmental Sciences of Ukraine, Kiev, Ukraine.

11 ³King's College London, London, United Kingdom.

12

13 * Corresponding author: N. Evangeliou (Nikolaos.Evangeliou@nilu.no)

14

15 **Abstract**

16 Highly unusual open fires burned in Western Greenland between 31 July and 21 August
17 2017, after a period of warm, dry and sunny weather. The fires burned on peat lands that
18 became vulnerable to fires by permafrost thawing. We used several satellite data sets to
19 estimate that the total area burned was about 2345 hectares. Based on assumptions of typical
20 burn depths and emission factors for peat fires, we estimate that the fires consumed a fuel
21 amount of about 117 kt C and emitted about 23.5 t of black carbon (BC) and 731 t of organic
22 carbon (OC) including 141 t of brown carbon (BrC). We used a Lagrangian particle
23 dispersion model to simulate the atmospheric transport and deposition of these species. We
24 find that the smoke plumes were often pushed towards the Greenland Ice Sheet by westerly
25 winds and thus a large fraction of the emissions (30%) was deposited on snow or ice covered
26 surfaces. The calculated deposition was small compared to the deposition from global
27 sources, but not entirely negligible. Analysis of aerosol optical depth data from three sites in
28 Western Greenland in August 2017 showed strong influence of forest fire plumes from
29 Canada, but little impact of the Greenland fires. Nevertheless, CALIOP lidar data showed that
30 our model captured the presence and structure of the plume from the Greenland fires. The
31 albedo changes and instantaneous surface radiative forcing in Greenland due to the fire
32 emissions were estimated with the SNICAR model and the uvspec model from the libRadtran
33 radiative transfer software package. We estimate that the maximum albedo change due to the
34 BC and BrC deposition was about 0.007, too small to be measured. The average instantaneous
35 surface radiative forcing over Greenland at noon on 31 August was 0.03–0.04 W m⁻², with
36 locally occurring maxima of 0.63–0.77 W m⁻² (depending on the studied scenario). The
37 average value is up to an order of magnitude smaller than the radiative forcing from other
38 sources. Overall, the fires burning in Greenland in summer of 2017 had little impact on the
39 Greenland Ice Sheet, causing a small extra radiative forcing. This was due to the – in a global
40 context – still rather small size of the fires. However, the very large fraction of the emissions
41 deposited on the Greenland Ice Sheet from these fires could contribute to accelerated melting
42 of the Greenland Ice Sheet if these fires become several orders of magnitude larger under
43 future climate.

44

Nikolaos Evangeliou 22/12/2018 08:17

Deleted: However, the very large fraction of the emissions deposited on the Greenland Ice Sheet makes these fires very efficient climate forcers on a per unit emission basis. If the expected future warming of the Arctic produces more severe fires in Greenland, this could indeed cause albedo changes and thus contribute to accelerated melting of the Greenland Ice Sheet. The fires burning in 2017 may be a harbinger of such future events.

55 **1 Introduction**

56 In August 2017 public media reported unprecedented fire events in Western Greenland
57 (BBC News, 2017; New Scientist Magazine, 2017). These events were documented with
58 airborne photographs (SERMITSIAQ, 2017) and satellite images (NASA, 2017b) and raised
59 public concerns about the effects of climate change and possible impacts of soot emissions on
60 ice melting. Historically, wildfires have occurred infrequently on Greenland, because three-
61 quarters of the island is covered by a permanent ice sheet and permafrost is found on most of
62 the ice-free land (Abdalati and Steffen, 2001). Permafrost, or permanently frozen soil, lies
63 under a several meters thick “active” soil layer that thaws seasonally. But in certain areas,
64 where the permafrost layer starts melting, it can expose peat, a material consisting of only
65 partially decomposed vegetation that forms in wetlands over the course of hundreds of years
66 or longer. Peatlands, also known as bogs and moors, are the earliest stage in the formation of
67 coal. Globally, the amount of carbon stored in peat exceeds that stored in vegetation and is
68 similar in size to the current atmospheric carbon pool (Turetsky et al., 2014). When peatlands
69 dry, they are often affected by fires burning into the peat layers. Peat fires are difficult to
70 extinguish and they often burn until all the organic matter is consumed. Smoldering peat fires
71 already are the largest fires on Earth in terms of their carbon footprint (Turetsky et al., 2014).
72 For Greenland, it has been suggested that degradation of peat will accelerate towards 2080
73 (Daanen et al., 2011) and that the area affected by the fires in August 2017 is particularly
74 vulnerable to permafrost thawing (Daanen et al., 2011).

75 Fires in the high northern latitudes release significant amounts of CO₂, CH₄, N₂O, black
76 carbon (BC) and organic carbon (OC) and their emissions are often transported into Arctic
77 regions (Cofer III et al., 1991; Hao et al., 2016; Hao and Ward, 1993; Shi et al., 2015). While
78 BC is the most strongly light-absorbing component of the atmospheric aerosol (Bond et al.,
79 2013), a portion of OC compounds has shown strong absorption towards shorter wavelengths
80 of the electromagnetic spectrum (UV), therefore defined as brown carbon (BrC) (Andreae and
81 Gelencsér, 2006; Chakrabarty et al., 2010). BC is formed by the incomplete combustion of
82 fossil fuels, biofuels, and biomass (Bond et al., 2013). BrC is emitted from smoldering fires or
83 solid fuel combustion (Bond, 2001), from pyrolysis of biomass (Mukai and Ambe, 1986) and
84 from biogenic emissions of humic substances (Limbeck et al., 2003). Due to their particulate
85 nature, both BC and OC are important for human health (Lelieveld et al., 2015) and climate
86 impacts (Myhre et al., 2013). BC has an atmospheric lifetime of 3–11 days (Bond et al.,
87 2013), while BrC lifetimes are estimated at 5–7 days (Jo et al., 2016), thus facilitating

88 transport over long distances (Forster et al., 2001; Stohl et al., 2006). BC, OC and BrC from
89 mid-latitude sources can thus reach remote areas such as the Arctic. They absorb solar
90 radiation in the atmosphere (Feng et al., 2013; Hansen and Nazarenko, 2004), have a
91 significant impact on cloud formation and also decrease surface albedo when deposited on ice
92 and snow and can accelerate melting processes (Hansen and Nazarenko, 2004; Wu et al.,
93 2016). This raises particular concerns about the effect of fires burning in the immediate
94 vicinity of the Greenland Ice Sheet. If a large fraction of the BC emitted by such fires is
95 deposited on the ice, these fires may be extremely effective in further enhancing the already
96 accelerating melting of the Greenland Ice Sheet (AMAP, 2017). BC, OC and BrC emissions
97 from such high latitude fires may also have a substantial effect on the albedo of sea ice.

98 Here we study transport and deposition of BC, OC and BrC over the Greenland Ice
99 Sheet from the fires that occurred in Western Greenland in August 2017, which likely
100 represent the largest fires that have occurred on Greenland in modern times (Figure S 1).
101 Since the fires occurred in an area entirely lacking ground-based observations, we use satellite
102 data and a Lagrangian atmospheric dispersion model for our study. Finally, we evaluate the
103 changes in the albedo of the Greenland Ice Sheet from the respective deposition of BC and
104 BrC and present instantaneous radiative forcing calculations for these two atmospheric
105 constituents released from the 2007 fires in Greenland.

106 2 Methods

107 2.1 Definition of burned area

108 Remote sensing has been useful for delineating fire perimeters, characterizing burn
109 severity and planning post-fire restoration activities in different regions. The use of satellite
110 imaging is particularly important for fire monitoring in remote areas due to difficult ground
111 access. The method that is presented in this section has been already used to calculate burned
112 area in the highly-contaminated radioactive forests of Chernobyl (Evangelidou et al., 2014,
113 2015, 2016). Coordinates of fire locations (hot spots) were downloaded from FIRMS (Fire
114 Information for Resource Management System) (NASA, 2017a). For the mapping of the
115 burned area, Sentinel 2A images were used. To delineate fire perimeters and define burn
116 severity precisely, we used Landsat 8 Operational Land Imager (OLI) (resolution: 30×30 m)
117 together with Sentinel 1A (resolution: 30×30 m) and Sentinel 2A images (resolution: 30×30
118 m) (see Table 1) by applying the differenced Normalized Burn Ratio (dNBR) (Key and
119 Benson, 2006):

Nikolaos Evangelidou 22/12/2018 08:33

Deleted: Figure S 1

Nikolaos Evangelidou 22/12/2018 08:33

Deleted: Table 1

122
$$dNBR = NBR_{pre-fire} - NBR_{post-fire} \quad (\text{Eq. 1})$$

123 Normalized burn ratios for pre- ($NBR_{pre-fire}$) and postfire ($NBR_{post-fire}$) images from
124 Sentinel 2A can be calculated using radiances for near- and shortwave infrared bands (bands 8
125 (NIR) and 12 (SWIR2) at 0.835 μm and 2.202 μm , respectively):

126
$$NBR = \frac{1000 \cdot (NIR - SWIR2)}{NIR + SWIR2} \quad (\text{Eq. 2})$$

127 The methodology of applying a dNBR index to assess the impact of fires has been used in
128 forests of the Northern and Western USA (French et al., 2008; Key and Benson, 2006) and
129 elsewhere (Escuin et al., 2008; Sunderman and Weisberg, 2011).

130 The burned severity mosaics were created using Sentinel 2A images corrected for
131 atmospheric scattering (see Chavez, 1988). Pre- and post-fire images were used to create
132 cloudless mosaics for the area where the Greenland fires burned. A Maximum Value
133 Composite (MVC) procedure (Holben, 1986) was used to select pixels from each band that
134 were not cloud covered and have a high value of Normalized Difference Vegetation Index
135 (NDVI). To avoid spurious burn severity values, manually delineated fire perimeters were
136 applied and all areas outside were classified as unburned. We have used common dNBR
137 severity levels (Key and Benson, 2006) that are presented in [Figure 1](#). The occasionally dense
138 cloud cover was the main obstacle in reconstructing fire dynamics. As an independent source
139 of information, active fires from MODIS satellite product MCD14DL (Giglio et al., 2003) are
140 plotted in Supplemental Information (SI) [Figure S 2](#).

141 2.2 Injection altitudes, assumptions on biomass consumption and emissions 142 factors

143 Injection heights into the atmosphere of the emitted smoke were simulated with version
144 2 of the Plume Rise Model (PRM) (Paugam et al., 2015) which is implemented in the Global
145 Fire Assimilation System (GFAS) emission inventory (Rémy et al., 2017). The model
146 (hereafter referred to as PRMv2) is a further development of PRM (Freitas et al., 2006, 2010)
147 and has already been used in previous studies of fire events (Evangelidou et al., 2015, 2016).
148 The model simulates a profile of smoke detrainment for every single fire, from which two
149 metrics are extracted: (i) a detrainment layer (i.e. where the detrainment rate is > 50% of its
150 global maximum) and (ii) an injection height (InjH, the top of the detrainment layer). Instead
151 of using the GFAS product, which uses the same statistics as in the PRMv2 InjH calculation,
152 we ran the model for every detected fire assuming a 6 h persistence and using the same
153 conversion factor as Kaiser et al. (2012) to estimate the biomass consumption. PRMv2 mass

Nikolaos Evangelidou 22/12/2018 08:33
Deleted: Figure 1

Nikolaos Evangelidou 22/12/2018 08:33
Deleted: Figure S 2

156 detrainment profiles are then time integrated and extracted at $1^\circ \times 1^\circ$ spatial resolution with a
157 500 m vertical mesh to estimate the 3D distribution of biomass burning smoke injection into
158 the atmosphere. [Figure S 3](#), (SI) shows for all fires recorded in the MODIS fire product
159 (Justice et al., 2002) during the fire period (31 July – 21 August 2017) the horizontal
160 distribution of the median height of the emitted smoke and its integration over the longitude
161 (right panel). Fires in Greenland showed a maximum injection height of around 2 km, but
162 according to PRMv2 the majority of the emissions (90%) remained below 800 m. Low
163 injection heights mostly inside the daytime planetary boundary layer are quite typical for
164 smoldering fires including peat fires (Ferguson et al., 2003) such as those burning in
165 Greenland (see below). For modeling the dispersion of BC, OC and BrC released from the
166 Greenland fires, the emission profiles from PRMv2 were ingested into the Lagrangian particle
167 dispersion model FLEXPART (see section 2.3).

168 Wildfires in boreal peatlands in the Canadian Arctic and in Alaska typically have
169 (shallow) burn depths of 1–10 cm and consume $20\text{--}30 \text{ t C ha}^{-1}$ (Benscoter and Wieder, 2003;
170 Shetler et al., 2008). The consumed carbon is often re-sequestered in 60–140 years after the
171 fire (Turetsky et al., 2011; Wieder et al., 2009). Given that fire return intervals can be as short
172 as 100–150 years in sub-humid continental peatlands (Wieder et al., 2009), and may exceed
173 2000 years in humid climates (Lavoie and Pellerin, 2007), northern peatlands are generally
174 resilient to wildfire (Magnan et al., 2012). For example, in peatlands of Northern Russia,
175 organic matter available for combustion has been estimated to be $121.8 \text{ t C ha}^{-1}$ for forested
176 lands and 21.3 t C ha^{-1} for non-forested lands (Smirnov et al., 2015). Accordingly, a severe
177 wildfire that burned within an afforested peatland in the Scottish Highlands during the
178 summer of 2006 had a mean depth of burn of $17.5 \pm 2.0 \text{ cm}$ (range: 1–54 cm) and a carbon loss
179 of $96 \pm 15 \text{ t C ha}^{-1}$ (Davies et al., 2013). In contrast, tropical peatlands can have deep burn
180 depths of 40–50 cm and release an average of $300\text{--}450 \text{ t C ha}^{-1}$ (Page et al., 2015; Reddy et
181 al., 2015). In the present study, we assume an average amount of organic fuel available for
182 combustion for the Greenland peat fires of August 2017 of 100 t C ha^{-1} , guided by values
183 suggested in Smirnov et al. (2015).

184 Estimation of the emissions of BC, OC and BrC, $E_{BC,OC,BrC}$ (kg), was based on the
185 following formula (Seiler and Crutzen, 1980; Urbanski et al., 2011) using the calculated
186 burned area A (ha) and a number of assumptions:

187
$$E_{BC,OC,BrC} = A \times FL \times \alpha \times EF \quad \text{Eq. 1}$$

Nikolaos Evangeliou 22/12/2018 08:33

Deleted: Figure S 3

189 Here, FL is the mass of the fuel available for combustion (kg C ha^{-1}); α is the dimensionless
190 combustion completeness, which was adopted from Hao et al. (2016) for litter and duff fuels
191 (50%). EF is the emission factor (kg kg^{-1}), which was assumed to be 0.20 g kg^{-1} for BC and
192 6.23 g kg^{-1} for OC for peatland fires (Akagi et al., 2011). Emission factors for BrC are rarely
193 reported, as BrC is only a fraction of OC. To our knowledge, the only reported emission
194 factors in the literature for BrC are from forest fires in the United States (Aurell and Gullett,
195 2013) estimated to be $1.0\text{--}1.4 \text{ g kg}^{-1}$ (value used here: 1.2 g kg^{-1}). Fuel consumption is
196 calculated as the product of burned area, fuel loading and combustion completeness
197 ($A \times FL \times \alpha$).

198 **2.3 Atmospheric modeling**

199 The emissions of BC, OC and BrC obtained from Eq. 1 were fed to the Lagrangian
200 particle dispersion model FLEXPART version 10.2 (Stohl et al., 2005) to simulate transport
201 and deposition. This model was originally developed for calculating the dispersion of
202 radioactive material from nuclear emergencies, but since then it has been used for many other
203 applications (e.g., Fang et al., 2014; Stohl et al., 2011, 2013). The model has a detailed
204 description of particle dispersion in the boundary layer and a convection scheme to simulate
205 particle transport in clouds (Forster et al., 2007). The model was driven by hourly $0.5^\circ \times 0.5^\circ$
206 operational analyses from the European Centre for Medium-Range Weather Forecasts
207 (ECMWF). Concentration and deposition fields were recorded in a global domain of $1^\circ \times 1^\circ$
208 spatial resolution with three hourly outputs. To capture the spatiotemporal variability of BC,
209 OC and BrC over the Greenland Ice Sheet, a nested domain with $0.05^\circ \times 0.05^\circ$ resolution was
210 used. The simulations accounted for wet and dry deposition, assuming a particle density of
211 1500 kg m^{-3} and a logarithmic size distribution with an aerodynamic mean diameter of
212 $0.25 \mu\text{m}$ and a standard deviation of 0.3 (Hu et al., 2018; Long et al., 2013). The wet
213 deposition scheme considers below-cloud and in-cloud scavenging separately based on cloud
214 liquid water and cloud ice content, precipitation rate and cloud depth from ECMWF, as
215 described in Grythe et al. (2017).

216 To compare BC and OC concentrations in Greenland due to the emissions of the
217 Greenland fires to those due to emissions occurring elsewhere, we used the so-called
218 “retroplume” mode of FLEXPART for determining the influence of other sources. For only a
219 few receptor points, this mode is computationally more efficient than forward simulations.
220 Computational particles were tracked 30 days back in time from four receptor regions:
221 Northwestern (-62°E to -42°E , 72°N to 83°N), Southwestern (-62°E to -42°E , 61°N to 72°N),

222 Northeastern (-42°E to -17°E, 72°N to 83°N) and Southeastern Greenland (-42°E to -17°E,
223 61°N to 72°N). The retroplume mode allowed identification of the origin of BC and OC
224 through calculated footprint emission sensitivities (often also called source-receptor
225 relationships) that express the sensitivity of the BC and OC surface concentrations at the
226 receptor to emissions on the model output grid. If these emissions are known, BC and OC
227 concentrations at the receptor can be calculated as the product of the emission flux and the
228 emission sensitivity. Also, detailed source contribution maps can be calculated, showing
229 which regions contributed to the simulated concentration. For the anthropogenic emissions,
230 we used the ECLIPSE (Evaluating the CLimate and Air Quality ImPacts of ShortlivEd
231 Pollutants) version 5 (Klimont et al., 2017) emission data set. For the biomass burning
232 emissions outside Greenland, we used operational CAMS GFAS emissions (Kaiser et al.,
233 2012). To our knowledge, actual gridded emissions of BrC are not yet available.

234 **2.4 Instantaneous radiative forcing (IRF) calculations**

235 The IRF of the emitted substances of interest were calculated using the uvspec model
236 from the libRadtran radiative transfer software package (<http://www.libradtran.org/doku.php>)
237 (Emde et al., 2016; Mayer and Kylling, 2005). The radiative transfer equation was solved in
238 the independent pixel approximation using the DISORT model in pseudo-spherical geometry
239 with improved treatment of peaked phase functions (Buras et al., 2011; Dahlback and
240 Stamnes, 1991; Stamnes et al., 1988). Radiation absorption by gases was taken from the Kato
241 et al. (1999) parameterization modified as described in the libRadtran documentation and
242 Wandji Nyamsi et al. (2015). External mixture of aerosols was assumed, i.e. BC and BrC
243 were treated in isolation of other aerosol types that may also have been present in the plume.
244 This assumption likely leads to underestimates of the radiative impacts, at least for BC
245 (Jacobson, 2001), in the atmosphere as coating, for example, can enhance its radiative effects.
246 However, these assumptions should have little impact on the more important albedo
247 calculations (see below). For snow-covered surfaces, deposited BC and BrC were assumed to
248 reside in the uppermost 5 mm. Below 5 mm the snow was assumed to be without any
249 impurities. The albedo of the snow was calculated with the SNICAR model
250 (<http://snow.engin.umich.edu/info.html>) in a two-layer configuration (Flanner et al., 2007,
251 2009).

252 The IRF was calculated for three scenarios: (a) BC only, (b) BC and BrC and (c) BC and
253 BrC, where all OC is considered to be BrC. The BC only scenario demonstrates the impact of
254 BC alone, while the two other scenarios provide an estimate of the additional impact of BrC

255 in the plume, with the last scenario considered to be a maximum estimate. We calculated both
256 the bottom of the atmosphere (BOA) and top of atmosphere (TOA) instantaneous radiative
257 forcing (IRF) due to the Greenland fires at $1^\circ \times 1^\circ$ resolution. The IRF includes both the effects
258 of BC and BrC in the atmosphere and deposited in snow. Note that the IRF does not include
259 any semi-direct nor indirect effects. We show IRF for cloudy conditions, which represents the
260 possible radiative effects of BC and BrC due to the 2017 fires with respect to the actual
261 meteorological situation. Liquid and ice water clouds were adopted from ECMWF.

262 **2.5 Remote sensing of the smoke plume**

263 To confirm the presence of the emitted substances from the Greenland fires and
264 elsewhere in the atmosphere over Greenland, we used the AERONET (AErosol RObotic
265 NETwork) data (Holben et al., 1998). AERONET provides globally distributed observations
266 of spectral aerosol optical depth (AOD), inversion products, and precipitable water in diverse
267 aerosol regimes. We chose data from three stations that were close to the 2017 fires and for
268 which cloud-free data exist for most of the simulated period, namely Kangerlussuaq
269 (50.62°W – 66.99°N), Narsarsuaq (45.52°W – 61.16°N) and Thule (68.77°W – 76.51°N). Their
270 locations are shown in [Figure S 2](#). We used Level 2.0 AOD data (fine and coarse mode AOD
271 at 500 nm and total AOD at 400 nm) from the AERONET version 3 direct-sun spectral
272 deconvolution algorithm (SDA version 4.1) product (downloaded on 20 July 2018) for the
273 simulated period (31 July to 31 August 2017).

274 To examine in particular the vertical depth of the smoke, we used data from the
275 CALIOP (Cloud-Aerosol Lidar with Orthogonal Polarization) lidar on the CALIPSO (Cloud-
276 Aerosol Lidar and Infrared Pathfinder Satellite Observations) platform (Winker et al., 2009).
277 CALIOP provides profiles of backscatter at 532 nm and 1064 nm, as well as the degree of the
278 linear polarization of the 532 nm signal. For altitudes below 8.3 km lidar profiles at 532 nm
279 are available with a vertical resolution of 30 m. We have utilized the level 1 data products
280 (version 3.40) of total attenuated backscatter at 532 nm. This signal responds to aerosols (like
281 BC, OC and BrC) as well as water and ice clouds, which in most cases can be distinguished
282 based on their differences in optical properties. The data were downloaded from the ICARE
283 Data and Services Center (<http://www.icare.univ-lille1.fr/>).

Nikolaos Evangeliou 22/12/2018 08:33

Deleted: Figure S 2

285 **3 Results**

286 **3.1 Indications of early permafrost degradation and fuel availability**

287 [Table 1](#), reports burned areas in August 2017 calculated for Greenland. In total, 2345
288 hectares burned between 31 July and 21 August 2017 ([Figure 1](#)). We estimate that about 117
289 kt of carbon were consumed by these fires. The area burned is not large compared to the
290 global area burned each year (464 million hectares), or the areas burned in boreal North
291 America (2.6 million hectares) or boreal Asia (9.8 million hectares) (Randerson et al., 2012),
292 but still highly unusual for Greenland.

293 It is not yet known how these fires started. Fires on carbon-rich soils can be initiated by
294 an external source, e.g. lightning, flaming wildfire and firebrand, or self-heating. The fires
295 burned relatively close to the town of Sisimut, so it is quite possible that humans started the
296 fires. Self-heating is another possibility as porous solid fuels can undergo spontaneous
297 exothermic reactions in oxidative atmospheres at low temperatures (Drysdale, 2011;
298 Restuccia et al., 2017b). This process starts by slow exothermic oxidation at ambient
299 temperature, causing a temperature increase, which is determined by the imbalance between
300 the rate of heat generation and the rate of heat losses (Drysdale, 2011). Fire initiated by self-
301 heating ignition is a well-known hazard for many natural materials (Fernandez Anez et al.,
302 2015; Restuccia et al., 2017a; Wu et al., 2015) and can also occur in natural soils (Restuccia
303 et al., 2017b). Southwestern Greenland was under anticyclonic influence during the last week
304 of July and according to the MODIS ESDIS worldview tool, direct sunshine occurred for
305 eight consecutive days before the fires started at the end of July 2017. It might be possible
306 that this long period of almost continuous insolation at these latitudes in July heated the soil
307 enough to self-ignite. In any case, the continuous sunshine had dried the soil, making it
308 susceptible to fire.

309 The fact that these fires were burning for about three weeks but spread relatively slowly
310 compared to above-ground vegetation fires indicates that the main fuel was probably peat.
311 The predominant vegetation in Western Greenland varies from carbon-rich *Salix glauca* low
312 shrubs (mean canopy height: 95 cm), mainly at low altitude south-facing slopes with deep
313 soils and ample moisture, to dwarf-shrubs and thermophilous graminoid vegetation (Arctic
314 steppe) at higher altitudes (Jedrzejek et al., 2013). In addition, the observed smoke was nearly
315 white, indicating damp fuel, such as freshly thawed permafrost, which produces smoke rich in
316 OC aerosol (Stockwell et al., 2016).

Nikolaos Evangeliou 22/12/2018 08:33

Deleted: Table 1

Nikolaos Evangeliou 22/12/2018 08:33

Deleted: Figure 1

319 Literally no fires should be expected in Greenland, since there is little available fuel as
320 it has been suggested by global models and validated by observations (Daanen et al., 2011;
321 Stendel et al., 2008); the only way to provide substantial amounts of fuel in Greenland is
322 permafrost degradation. However, it has been suggested that significant permafrost loss in
323 Greenland may occur only by the end of the 21st century (Daanen et al., 2011; Stendel et al.,
324 2008). The fires in 2017 might indicate that significant permafrost degradation has occurred
325 sooner than expected.

326 3.2 Transport and deposition of BC in Greenland

327 We estimate that about 23 t of BC and 731 t of OC, including 141 t of BrC, were
328 released from the Greenland fires in August 2017 (Table 1). According to the FLEXPART
329 model simulations, these emissions were transported and deposited as shown in Figure 2. Due
330 to the low injection altitude of the releases within the boundary layer, transport was relatively
331 slow and thus the emitted substances initially remained quite close to their source. Slow
332 transport was also favored by mostly anticyclonic influence during the first half of August. It
333 seems that even though katabatic winds from the Greenland Ice Sheet occasionally
334 transported the plume westwards, most of the time the large-scale circulation pushed the
335 plume back towards Greenland (see SI animations). Consequently, a large fraction of the
336 emitted substances were deposited in Southwestern Greenland. On 3 August a small portion
337 of the emitted BC, OC and BrC (0.5 t, 16.1 t and 3.1 t, respectively) were lifted higher into
338 the atmosphere and were transported to the east and deposited in the middle of the Ice Sheet
339 over the course of the following two days (4 and 5 August). From 5 to 8 August, when the
340 fires were particularly intense, the emitted aerosols were transported to the south, where they
341 were deposited at the southern part of the Ice Sheet and close to the coastline. At the same
342 time, another branch of the plume was moving to the north depositing BC, OC and BrC over
343 Greenland's western coastline up to 80°N. Around 10 August, the plume circulated north- and
344 then eastwards in the northwestern sector of the anti-cyclone and the emitted aerosols were
345 deposited to the northern part of the Ice Sheet until 13 August. From around 16 August, a
346 cyclone approached from the northwest and the smoke was briefly transported directly
347 eastwards along the southern edge of the cyclone (see SI animations). Strong rain associated
348 with the cyclone's frontal system appears to have largely extinguished the fire by 17 or 18
349 August, although smaller patches may have continued smoldering for a few more days before
350 they also died out. The exact fire behavior after 16 August is difficult to determine because of

Nikolaos Evangeliou 22/12/2018 08:33

Deleted: Table 1

Nikolaos Evangeliou 22/12/2018 08:33

Deleted: Figure 2

353 frequent dense cloud cover. However, satellite imagery on 21 August shows no smoke
354 anymore in the area where the fires had burned.

355 The total deposition of BC, OC and BrC from the fires in Greenland was estimated to
356 be 9 t, 280 t and 54 t, respectively, or about 39% of the total emissions. About 7 t of BC, 218 t
357 of OC and 42 t of BrC were deposited on snow or ice covered surfaces, which is equivalent to
358 30% of the total emissions. Most of the rest was deposited in the Baffin Bay between
359 Greenland and Canada and in the Atlantic Ocean. With 30% of the emissions deposited on
360 snow or ice surfaces, Greenland fires may have a relatively large efficiency for causing
361 albedo changes on the Greenland Ice Sheet.

362 By comparison, the respective BC deposition on snow and ice surfaces over Greenland
363 from global emissions of BC (from ECLIPSEv5) was only 0.4% (39 kt) of the total emissions.
364 Even the total deposition of BC in the Arctic (>67°N) was only about 3% (215 kt). This
365 indicates the high relative potential of Greenland fires to pollute the cryosphere (on a per unit
366 emission basis), likely also giving them a particularly high radiative forcing efficiency.
367 Considering that the projected rise of Greenland temperatures is expected to result in further
368 degradation of the permafrost (Daanen et al., 2011) and, hence, likely resulting in more and
369 larger peat fires on Greenland, this constitutes a potentially important climate feedback which
370 could accelerate melting of the glaciers and ice sheet of Greenland and enhance Arctic
371 warming.

372 We also calculated the concentration of the deposited carbon aerosols in Greenland
373 snow (Figure 3) by taking the ratio of deposited quantities and the amount of water deposited
374 by rain or snowfall during the same time period (31 July to 31 August 2017). As expected,
375 snow concentrations show the same general patterns as the simulated deposition with the
376 highest concentrations obtained close to the source (western side of Greenland). High snow
377 concentrations were also computed in some regions of the Ice Sheet due to relatively intense
378 precipitation events. By contrast, dry deposition (example for BC) over the Ice Sheets was
379 low (Figure S 4). Dry deposition was responsible for a major fraction of the deposition only in
380 regions where the plume was transported during dry weather, and in most of these regions
381 total deposition was low. A notable exception is the region close to the fires, where dry
382 deposition was relatively important due to the generally dry weather when the fires were
383 burning. It can be also ascribed to the fact that dry deposition occurs in the quasi-laminar sub-
384 layer close to the surface. A fraction of the aerosols can be quickly deposited close to the
385 sources before they are transported to higher altitudes and away from the sources (Bellouin

Nikolaos Evangeliou 22/12/2018 08:33

Deleted: Figure 3

Nikolaos Evangeliou 22/12/2018 08:33

Deleted: Figure S 4

388 and Haywood, 2014). The average calculated snow concentration of BC on the Ice Sheet was
389 estimated to be $<1 \text{ ng g}^{-1}$, but in some areas snow concentrations reached up to 3 ng g^{-1} . These
390 higher values are substantial considering that measured concentrations of BC in snow
391 typically range up to 16 ng g^{-1} in most of Greenland (Doherty et al., 2010) or from 1 – 17
392 ng g^{-1} in summer 2012 and 3–43 ng g^{-1} in summer 2013 (Polashenski et al., 2015) and up to 15
393 ppb C (ng g^{-1}) during preindustrial times (from 1740 to 1870) on average (Legrand et al.,
394 2016). OC concentrations in snow were 2 ng g^{-1} (ppb C), on average, with local maxima of 10
395 ng g^{-1} . They are lower than those measured in snow over several places in Antarctica (23–928
396 ppb C) (Antony et al., 2011; Grannas et al., 2004; Legrand et al., 2013; Lyons et al., 2007), in
397 Greenland (400–580 ppb C) (Grannas et al., 2004) or in the Alps (70–304 ppb C) (Legrand et
398 al., 2013). Snow BrC was estimated to be even less; though, to our knowledge, no available
399 measurements exist in the relevant literature so far.

400 It has been reported that the size of rapidly coagulated aerosol particles produced by
401 different types of fires ranges between 0.1 to $10 \text{ }\mu\text{m}$, but more than 90% of the mass lies
402 between 0.1 and $1 \text{ }\mu\text{m}$ (e.g., Conny and Slater, 2002; Long et al., 2013; Zhuravleva et al.,
403 2017 and many others). Therefore, we simulated the Greenland fires with an aerodynamic
404 mean diameter of $0.25 \text{ }\mu\text{m}$ for BC, OC and BrC and a logarithmic standard deviation of 0.3
405 (see section 2.3), because all these substances have more or less the same lifetimes (Bond et
406 al., 2013; Jo et al., 2016; Lim et al., 2003). To examine the sensitivity of deposition in the
407 Greenland Ice Sheet from the Greenland fires of 2017 to the particle size distribution used in
408 the model, we simulated the same event for particles with aerodynamic mean diameters of
409 0.1, 0.25, 0.5, 1, 2, 4 and $8 \text{ }\mu\text{m}$ and calculated the relative standard deviation of deposition
410 normalized against the aerodynamic mean diameter of $0.25 \text{ }\mu\text{m}$ that was our basic
411 assumption. The results are shown in [Figure S 5](#), for BC. The use of different size distributions
412 for the BC particles produced from the 2017 fires created a relative uncertainty on the
413 deposited mass of BC in the Greenland Ice Sheet, which ranges from 10%–30% in 86% of the
414 Sheet's surface to up to 50% in the rest of the Sheet's surface. As expected, the calculated
415 uncertainty is sensitive to the use of larger particles for BC; though BC particles larger than 1
416 μm are rather rare in peat fires (Hosseini et al., 2010; Leino et al., 2014).

417 3.3 Impact from other emissions in the Northern Hemisphere

418 In summertime 2017, intense wildfires were reported in British Columbia, Western
419 Canada (NASA, 2017c), and fires also burned at mid latitudes in Eurasia, as is typical during
420 spring and summer (Hao et al., 2016). Previous studies of wildfires have shown that the

Nikolaos Evangeliou 22/12/2018 08:33

Deleted: Figure S 5

422 produced energy can be sufficient to loft smoke above the boundary layer by supercell
423 convection (Fromm et al., 2005) even up to stratospheric altitudes (Leung et al., 2007). As a
424 result, emitted aerosols can become subject to long-range transport over long distances
425 (Forster et al., 2001; Stohl et al., 2007). To examine the impact of these fires in Greenland,
426 average footprint emission sensitivities were calculated for four compartments of Greenland
427 (Northwestern, Southwestern, Northeastern and Southeastern Greenland) for the period 31
428 July to 31 August 2017 and the results are shown in [Figure S 6](#), together with the active fires
429 in the Northern Hemisphere from 10 July to 31 August 2017 adopted from the MODIS
430 satellite product (MCD14DL) (Giglio et al., 2003). As can be seen in [Figure S 6](#), fires in
431 Alaska and in Western Canada might have affected BC, OC and BrC concentrations in
432 Greenland, as the corresponding emission sensitivities are the highest in North America. On
433 the contrary, emissions from fires in Eurasia seem to have affected Greenland less.

Nikolaos Evangeliou 22/12/2018 08:33

Deleted: Figure S 6

Nikolaos Evangeliou 22/12/2018 08:33

Deleted: Figure S 6

434 Using gridded emissions for BC and OC, the contribution of both biomass burning and
435 anthropogenic sources to surface concentrations in the four different regions over Greenland
436 (Northwestern, Northeastern, Southwestern and Southeastern Greenland, [Figure S 7](#)) was
437 calculated (see section 2.3). Fires affected the northern part of Greenland more than the
438 southern part with an average BC concentration of about 30 ng m^{-3} , almost twice the
439 respective average for Southern Greenland ($\approx 16 \text{ ng m}^{-3}$). OC simulated concentrations were
440 much higher than those of BC with an average concentration of 945 ng m^{-3} in North
441 Greenland, while the respective concentrations in the southern part were about 490 ng m^{-3} .
442 About one third of BC and OC originated from wildfires in Eurasia and the rest from North
443 America where the year 2017 appears to have been a particularly high fire year. The
444 anthropogenic contribution to surface concentrations of BC and OC over Greenland was
445 between 14% to 50% of the total contribution from all biomass burning sources ([Figure S 7](#)),
446 similar to what has been suggested previously for the Arctic in summer (Winiger et al., 2017).
447 The anthropogenic contribution is larger in Southern Greenland than in Northern Greenland,
448 due to the shorter distance from the main emission areas of North America and Western
449 Europe, but it remains much lower than the biomass burning contribution. The concentrations
450 of BC and OC that are calculated for the studied fire period (31 July to 31 August 2017) are
451 relatively high compared to those reported previously. For instance, von Schneidemesser et al.
452 (2009) observed an annual average BC concentration of 20 ng m^{-3} at Summit (Greenland) in
453 2006, while Massling et al. (2015) reported a summer average BC concentration of 11 ng m^{-3}
454 at station Nord (Greenland) between May 2011 and August 2013. As regards to OC, average

Nikolaos Evangeliou 22/12/2018 08:33

Deleted: Figure S 7

Nikolaos Evangeliou 22/12/2018 08:33

Deleted: Figure S 7

459 concentrations of its water soluble part were measured in 2006 between 194 and 730 ng m⁻³ in
460 Summit, Greenland (Anderson et al., 2008) showing a large decreasing trend compared to
461 previous years (Dibb et al., 2002). We attribute this difference in the calculated concentrations
462 to more active fires during 2017 in Greenland than in previous years (see [Figure S 1](#)).

463 As an example of the importance of Northern Hemispheric biomass burning emissions
464 for the air over Greenland, we present time-series of surface BC concentrations in
465 Northwestern, Northeastern, Southwestern and Southeastern Greenland from the fires in
466 Greenland and from all the other wildfire emission sources occurring outside Greenland
467 (North Hemisphere) for the same period of time ([Figure 4](#)). The calculated dosages
468 (concentrations summed over a specific time period) for the same time period were also
469 computed. The fires in Greenland affected mainly its western part with concentrations that
470 reached up to 4.8 ng m⁻³ (Southwestern Greenland on 10 August) and 4.4 ng m⁻³
471 (Northwestern Greenland on 12 August), while BC concentrations in the eastern part
472 remained significantly lower ([Figure 4](#)). These concentrations are substantial considering that
473 the observed surface BC concentrations in Greenland in summer are usually below 20 ng m⁻³
474 (Massling et al., 2015). Surface BC due to wildfires occurring outside Greenland was also low
475 most of the time in the studied period (up to 10 ng m⁻³ at maximum) except for a large peak
476 between 19 and 23 August that mainly affected Northern Greenland ([Figure 4](#)). The
477 concentrations during this episodic peak were as high as 27 ng m⁻³. During the same period,
478 the contribution from anthropogenic emissions was also a few ng m⁻³ ([Figure 4](#)). BC dosages
479 for the simulation period (31 July – 10 August 2017) in Western Greenland due to the
480 Greenland fires were about one order of magnitude smaller than dosages from fires elsewhere
481 but of the same order of magnitude as BC originating from anthropogenic emissions.

482 4 Discussion

483 4.1 An evaluation attempt

484 There are few observations available that can be used to [evaluate](#) our model results. We
485 use the AERONET and CALIOP data for some qualitative comparisons. We present only BC
486 here, but similar plots can be generated for OC, considering that we used the same scavenging
487 coefficients as for BC to represent the similar lifetimes of BC and OC (Bond et al., 2013; Jo
488 et al., 2016; Lim et al., 2003). Contours of simulated vertical distribution of BC and column-
489 integrated simulated BC from fires inside and outside Greenland are plotted together with
490 time-series of measured AOD (fine and coarse mode AOD at 500 nm and total AOD at 400

Nikolaos Evangeliou 22/12/2018 08:33

Deleted: Figure S 1

Nikolaos Evangeliou 22/12/2018 08:33

Deleted: Figure 4

Nikolaos Evangeliou 22/12/2018 08:33

Deleted: Figure 4

Nikolaos Evangeliou 22/12/2018 08:33

Deleted: Figure 4

Nikolaos Evangeliou 22/12/2018 08:33

Deleted: Figure 4

Nikolaos Evangeliou 22/12/2018 08:23

Deleted: validation

Nikolaos Evangeliou 22/12/2018 08:24

Deleted: validate

498 | nm) for the AERONET stations Kangerlussuaq, Narsarsuaq and Thule (Figure 5). It can be
499 | seen that observed AOD variations were in very good agreement with the variation of
500 | simulated column-integrated BC from fires outside Greenland (mainly in Canada), confirming
501 | that the transport of these fire plumes was well captured by FLEXPART. Good examples are
502 | the peaks at Kangerlussuaq on 24 August, at Narsarsuaq on 19 August and at Thule on 21
503 | August (Figure 5) that are attributed to the Canadian fires. The simulated contribution of the
504 | Greenland fires to simulated BC burdens was negligible by comparison, except at
505 | Kangerlussuaq in the beginning of August when the Greenland fire emissions were the
506 | highest. This station is less than 100 km away from where the fires burned, but not in the
507 | main direction of the BC plume transport. It seems the period of simulated fire influence
508 | corresponds to a small increase of the observed AOD values of up to 20% (Figure 5).

509 | To evaluate the smoke plume's vertical extent, we used the CALIOP data. These data
510 | were only available from 5 August 2017 onward and frequent dense cloud cover inhibited
511 | lidar observations at the altitudes below the clouds. High aerosol backscatter was only found
512 | in the close vicinity of the fires. Figure 6a shows NASA's ESDIS view of the plume on 14
513 | August 2017 at 6 UTC (available: [https://worldview.earthdata.nasa.gov/?p=geographic&l=MODIS_Aqua_CorrectedReflectance_TrueColor\(hidden\),MODIS_Terra_CorrectedReflectance_TrueColor,MODIS_Fires_Terra,MODIS_Fires_Aqua,Reference_Labels\(hidden\),Reference_Features,Coastlines&t=2017-08-14&z=3&v=-54.13349998138993,66.35888052399868,-50.32103113049877,69.08420005412792](https://worldview.earthdata.nasa.gov/?p=geographic&l=MODIS_Aqua_CorrectedReflectance_TrueColor(hidden),MODIS_Terra_CorrectedReflectance_TrueColor,MODIS_Fires_Terra,MODIS_Fires_Aqua,Reference_Labels(hidden),Reference_Features,Coastlines&t=2017-08-14&z=3&v=-54.13349998138993,66.35888052399868,-50.32103113049877,69.08420005412792)), where
514 | a clear smoke signal was recorded. A CALIOP overpass through the edge of the plume allows
515 | studying its vertical structure. Increased attenuated backscatter is found below ~1.5 km above
516 | sea level between 52°E and 51°E (Figure 6b; black line denotes the orography). Figure 6c
517 | (red line), shows that the CALIOP overpass transects directly the simulated plume of the
518 | Greenland fires. Notice that the simulated plume also agrees very well with the smoke as seen
519 | in NASA's ESDIS picture (Figure 6a). The vertical distribution of simulated BC as a function
520 | of longitude is illustrated in Figure 6d. It corresponds very well to the vertical distribution of
521 | aerosols observed by CALIOP (Figure 6b). In particular, the smoke resides at altitudes below
522 | 1.5 km and at exactly the same location both in the simulations and observations.

527 | 4.2 Instantaneous radiative forcing and albedo effects

528 | BOA IRF due to (a) BC only, (b) BC and BrC and (c) BC and BrC when all OC was
529 | assumed to be BrC (extreme scenario) for noon on 31 August 2017 is depicted in Figure 7a-c.
530 | This day is shown because almost all the aerosols emitted by the fires had been deposited,

Nikolaos Evangeliou 22/12/2018 08:33

Deleted: Figure 5

Nikolaos Evangeliou 22/12/2018 08:33

Deleted: Figure 5

Nikolaos Evangeliou 22/12/2018 08:33

Deleted: Figure 5

Nikolaos Evangeliou 22/12/2018 08:24

Deleted: validate

Nikolaos Evangeliou 22/12/2018 08:33

Deleted: Figure 6

Nikolaos Evangeliou 22/12/2018 08:33

Deleted: Figure 6

Nikolaos Evangeliou 22/12/2018 08:33

Deleted: Figure 6

Nikolaos Evangeliou 22/12/2018 08:33

Deleted: Figure 6

Nikolaos Evangeliou 22/12/2018 08:33

Deleted: Figure 6

Nikolaos Evangeliou 22/12/2018 08:33

Deleted: Figure 6

Nikolaos Evangeliou 22/12/2018 08:33

Deleted: Figure 7

542 thus giving a high IRF via albedo reduction due to snow contamination. The IRF is the largest
543 over ice close to the fire site and at locations where relatively large amounts of BC and BrC
544 were deposited. For BC only, the maximum BOA (TOA) IRF is 0.63 W m^{-2} (0.59 W m^{-2}),
545 and the average 0.03 W m^{-2} (0.03 W m^{-2}). Including BrC slightly increases the maximum
546 BOA (TOA) IRF to 0.65 W m^{-2} (0.61 W m^{-2}), while the change in the average IRF values is
547 negligible. For the extreme BrC scenario, the maximum BOA (TOA) IRF is 0.77 W m^{-2} (0.71
548 W m^{-2}) and the average 0.04 W m^{-2} (0.06 W m^{-2}). So, including BrC in our analysis increases
549 BOA IRF by only 20% even for the extreme scenario.

550 The IRF depends on the optical properties of the smoke from the fire, which are not
551 known. Hence, a sensitivity analysis was performed where the single scattering albedo (SSA)
552 was perturbed in contrast to a “medium case” (Figure S 8a) that was adopted from the
553 SNICAR model (Flanner et al., 2007, 2009) and has been used for the discussion in the
554 previous paragraph. To estimate the uncertainty due to the choice of BC optical properties,
555 additional calculations were made by scaling the SSA (red solid lines in Figure S 8a). The
556 choices of these scaled SSA values were based on the SSA reported for various modified
557 combustion efficiencies (MCE) by Pokhrel et al. (2016). Pokhrel et al. (2016) reported an
558 MCE of 0.9 for peat land. As such, our adopted SSA may be considered low (compare black
559 solid line and red line with upward triangles). Figure S 8b shows the IRF as BC is deposited
560 for the three cases. It suggests that the IRF ranges between 40% and 130% of our above-
561 assumed medium-case values for realistic variation of the aerosol optical properties.

562 Figure 7d depicts the temporal behaviour of the cloudy TOA IRF averaged over
563 Greenland (daily averages) for BC only (red line), for BC and BrC (blue line) and for BC and
564 BrC, when all OC is assumed to be BrC (black line, extreme case scenario). The daily
565 averaged IRF is seen to increase as the plume from the fires spreads out and starts to decline
566 after the fires were extinguished at the end of the month. The fact that the reduction towards
567 end of August is relatively slow is caused by the effect of the albedo reduction, which persists
568 until clean snow covers the polluted snow. Overall, albedo reduction dominates the total IRF
569 averaged over Greenland for the period of study contributing between 85% (in the beginning
570 of the study period) to 99% (at the end of the study period) and increasing in relative
571 importance with time as atmospheric BC and BrC are removed. The largest IRF differences
572 between the BC only case IRF and the two BC+BrC cases occur when there is still smoke in
573 the air and the lowest IRF differences occur after August 15th. This indicates that BrC is most
574 important for the IRF when it is airborne, even in the extreme scenario. However, for the

Nikolaos Evangeliou 22/12/2018 08:33

Deleted: Figure S 8

Nikolaos Evangeliou 22/12/2018 08:33

Deleted: Figure S 8

Nikolaos Evangeliou 22/12/2018 08:33

Deleted: Figure S 8

Nikolaos Evangeliou 22/12/2018 08:33

Deleted: Figure 7

579 latter, the impact is also large after August 15th due to a further albedo decrease of about
580 0.001 compared to the case where only BC was considered.

581 According to Hansen et al. (2005) the TOA IRF of BC approximates the adjusted RF as
582 reported by Myhre et al. (2013). In their Table 8.4, Myhre et al. (2013) estimated the global
583 averaged RF due to BC between the years 1750 and 2011 to be +0.40 (+0.05 to +0.80) W m⁻².
584 Skeie et al. (2011) estimated a global mean radiative forcing of 0.35 W m⁻² due to fossil fuel
585 and biofuel increases between 1750 and 2000. For Greenland, Skeie et al. (2011) found the
586 RF to be less than about 0.2 W m⁻². This number may be compared to our area averaged IRF
587 estimate due to the Greenland fire. For cloudy conditions the TOA IRF over Greenland due to
588 the Greenland fires is about a factor 4 to 10 smaller compared with the RF over Greenland
589 due to BC from all global anthropogenic sources reported in Skeie et al. (2011).

590 The albedo reduction at 550 nm for the three scenarios (BC only, BC+BrC and BC+BrC
591 extreme) is shown in [Figure 7e-g](#). The maximum albedo change is about 0.006 when only BC
592 was considered. Adding BrC from the most extreme scenario, the maximum albedo change
593 was calculated as 0.007 This albedo change has an impact on IRF, but it is too small to be
594 measured by satellites. For example, MODIS albedo estimates have been compared to in situ
595 albedo measurements in Greenland by Stroeve et al. (2005). They found that the root mean
596 square error between MODIS and in situ albedo values was ±0.04 for high quality flagged
597 MODIS albedo retrievals. Unmanned Aerial Vehicle (UAV) measurements over Greenland
598 made by Burkhart et al. (2017) have uncertainties of similar magnitude. Also, Polashenski et
599 al. (2015) reported that the albedo reduction due to aerosol impurities on the Greenland Ice
600 Sheet in 2012–2014 period is relatively small (mean 0.003), though episodic aerosol
601 deposition events can reduce albedo by 0.01–0.02. The albedo changes due to BC and BrC
602 from the Greenland fires are generally an order of magnitude smaller ([Figure 7e-g](#)) and thus
603 too small to be detected by present UAV and satellite instruments and retrieval methods
604 (Warren, 2013).

605 5 Conclusions

606 We studied atmospheric transport, deposition and impact of BC, BrC and OC emitted as
607 a result of unusual open fires burning in Greenland between 31 July and 21 August 2017. Our
608 conclusions can be summarized below:

- 609 • The fires burned on peat lands that became vulnerable by permafrost thawing. The region
610 where the fires burned was identified previously as being susceptible to permafrost

Nikolaos Evangeliou 22/12/2018 08:33
Deleted: Figure 7

Nikolaos Evangeliou 22/12/2018 08:33
Deleted: Figure 7

613 melting; however, large-scale melting was expected to occur only towards the end of the
614 21st century. The 2017 fires show that at least in some locations substantial permafrost
615 thawing is already occurring now.

616 • The total area burned was about 2345 hectares. We estimate that the fires consumed a fuel
617 amount of about 117 kt C and emitted about 23.5 t of BC and 731 t of OC including 141 t
618 of BrC.

619 • The Greenland fires were small compared to fires burning at the same time in North
620 America and Eurasia, but a large fraction of BC, OC and BrC emissions (30%) was
621 deposited on the Greenland Ice Sheet.

622 • Measurements of aerosol optical depth at three sites in Western Greenland in August 2017
623 were strongly influenced by forest fires in Canada burning at the same time, but the
624 Greenland fires had an observable impact doubling the column-integrated BC
625 concentrations at the closest station.

626 • A comparison of the simulated BC releases in FLEXPART with the vertical cross-section
627 of total attenuated backscatter (at 532 nm) from CALIOP lidar showed that the
628 spatiotemporal evolution and particularly the top height of the plume was captured by the
629 model.

630 • We estimate that the maximum albedo change due to the BC deposition from the
631 Greenland fires was about 0.006, whereas adding deposited BrC increases albedo to 0.007
632 at maximum, which is too small to be measured. The average instantaneous BOA radiative
633 forcing over Greenland at noon on 31 August was between 0.03–0.04 W m⁻² for the three
634 scenarios (BC only, BC+BrC and BC+BrC extreme), with locally occurring maxima of
635 0.63 W m⁻², 0.65 W m⁻² and 0.77 W m⁻², respectively. The average value when only BC
636 was considered is up to an order of magnitude smaller than the radiative forcing due to BC
637 from other sources.

638 • We conclude that the fires burning in Greenland in summer of 2017 had small impact on
639 the Greenland Ice Sheet, causing almost negligible extra radiative forcing. This was due to
640 the – in a global context – still rather small size of the fires.

641 The very large fraction of the emissions deposited on the Greenland Ice Sheet from
642 these fires (30% of the emissions) could contribute to accelerated melting in Greenland if such
643 fires become more severe under future climate.

644 The very large fraction of the emissions deposited on the Greenland Ice Sheet makes
645 these fires very efficient climate forcers on a per unit emission basis. Thus, while the fires in

Nikolaos Evangeliou 22/12/2018 08:26
Deleted: on

Nikolaos Evangeliou 22/12/2018 08:21
Deleted: (30% of the emissions)

648 2017 were still relatively small on a global scale, if the expected future warming of the Arctic
649 (IPCC, 2013) produces more and larger fires in Greenland (Keegan et al., 2014), this could
650 indeed cause substantial albedo changes and thus contribute to accelerated melting of the
651 Greenland Ice Sheet.

652

653 *Data availability.* All data used for the present publication can be obtained from the
654 corresponding author upon request.

655

656 *Competing financial interests.* The authors declare no competing financial interests.

657

658 *Acknowledgements.* This study was partly supported by the Arctic Monitoring and
659 Assessment Programme (AMAP) and was conducted as part of the Nordic Centre of
660 Excellence eSTICC (Nordforsk 57001). We acknowledge the use of imagery from the NASA
661 Worldview application (<https://worldview.earthdata.nasa.gov/>) operated by the
662 NASA/Goddard Space Flight Center Earth Science Data and Information System (ESDIS)
663 project. We thank Brent Holben and local site managers for their effort in establishing and
664 maintaining the AERONET sites used in this investigation. We thank NASA/CNES engineers
665 and scientists for making CALIOP data available. The lidar data were downloaded from the
666 ICARE Data and Service Center.

667

668 *Author contributions.* NE performed the simulations, analyses, wrote and coordinated the
669 paper. AK performed the radiation calculations and wrote parts of the paper. VM and SZ
670 performed GIS analysis for the burned area calculations. RP made all the runs for the
671 injection height calculations using the PRMv2 model. KS analysed satellite data for AOD and
672 CALIOP, SE and AS commented and coordinated the manuscript. All authors contributed to
673 the final version of the manuscript.

674

675 **References**

- 676 Abdalati, W. and Steffen, K.: Greenland Ice Sheet melt extent:1979-1999, *J. Geophys. Res.*
677 *Atmos.*, 106(D24), 33983–33988, doi:10.1029/2001JD900181, 2001.
- 678 Akagi, S. K., Yokelson, R. J., Wiedinmyer, C., Alvarado, M. J., Reid, J. S., Karl, T., Crounse, J.
679 D. and Wennberg, P. O.: Emission factors for open and domestic biomass burning for use
680 in atmospheric models, *Atmos. Chem. Phys.*, 11(9), 4039–4072, doi:10.5194/acp-11-
681 4039-2011, 2011.
- 682 AMAP: Snow, Water, Ice and Permafrost. Summary for Policy-makers, Arctic Monitoring
683 and Assessment Programme (AMAP), Oslo, Norway. [online] Available from:
684 <https://www.amap.no/documents/doc/Snow-Water-Ice-and-Permafrost.-Summary->

685 for-Policy-makers/1532 (Accessed 27 November 2017), 2017.

686 Anderson, C. H., Dibb, J. E., Griffin, R. J., Hagler, G. S. W. and Bergin, M. H.: Atmospheric
687 water-soluble organic carbon measurements at Summit, Greenland, *Atmos. Environ.*,
688 42(22), 5612–5621, doi:10.1016/j.atmosenv.2008.03.006, 2008.

689 Andreae, M. O. and Gelencsér, A.: Black carbon or brown carbon? The nature of light-
690 absorbing carbonaceous aerosols, *Atmos. Chem. Phys.*, 6(3), 3419–3463,
691 doi:10.5194/acpd-6-3419-2006, 2006.

692 Antony, R., Mahalinganathan, K., Thamban, M. and Nair, S.: Organic carbon in antarctic
693 snow: Spatial trends and possible sources, *Environ. Sci. Technol.*, 45(23), 9944–9950,
694 doi:10.1021/es203512t, 2011.

695 Aurell, J. and Gullett, B. K.: Emission factors from aerial and ground measurements of
696 field and laboratory forest burns in the southeastern U.S.: PM_{2.5}, black and brown
697 carbon, VOC, and PCDD/PCDF, *Environ. Sci. Technol.*, 47(15), 8443–8452,
698 doi:10.1021/es402101k, 2013.

699 BBC News: “Unusual” Greenland wildfires linked to peat, [online] Available from:
700 <http://www.bbc.com/news/science-environment-40877099> (Accessed 6 September
701 2017), 2017.

702 Bellouin, N. and Haywood, J.: *Aerosols: Climatology of Tropospheric Aerosols*, Second
703 Edi., Elsevier., 2014.

704 Benscoter, B. W. and Wieder, R. K.: Variability in organic matter lost by combustion in a
705 boreal bog during the 2001 Chisholm fire, *Can. J. For. Res.*, 33(12), 2509–2513,
706 doi:10.1139/x03-162, 2003.

707 Bond, T. C.: Spectral dependence of visible light absorption by carbonaceous particles
708 emitted from coal combustion, *Geophys. Res. Lett.*, 21(21), 4075–4078,
709 doi:10.1029/2001GL013652, 2001.

710 Bond, T. C., Doherty, S. J., Fahey, D. W., Forster, P. M., Berntsen, T., Deangelo, B. J., Flanner,
711 M. G., Ghan, S., Kärcher, B., Koch, D., Kinne, S., Kondo, Y., Quinn, P. K., Sarofim, M. C.,
712 Schultz, M. G., Schulz, M., Venkataraman, C., Zhang, H., Zhang, S., Bellouin, N., Guttikunda,
713 S. K., Hopke, P. K., Jacobson, M. Z., Kaiser, J. W., Klimont, Z., Lohmann, U., Schwarz, J. P.,
714 Shindell, D., Storelvmo, T., Warren, S. G. and Zender, C. S.: Bounding the role of black
715 carbon in the climate system: A scientific assessment, *J. Geophys. Res. Atmos.*, 118(11),
716 5380–5552, doi:10.1002/jgrd.50171, 2013.

717 Buras, R., Dowling, T. and Emde, C.: New secondary-scattering correction in DISORT with
718 increased efficiency for forward scattering, *J. Quant. Spectrosc. Radiat. Transf.*, 112(12),
719 2028–2034, doi:10.1016/j.jqsrt.2011.03.019, 2011.

720 Chakrabarty, R. K., Moosmüller, H., Chen, L. W. A., Lewis, K., Arnott, W. P., Mazzoleni, C.,
721 Dubey, M. K., Wold, C. E., Hao, W. M. and Kreidenweis, S. M.: Brown carbon in tar balls
722 from smoldering biomass combustion, *Atmos. Chem. Phys.*, 10(13), 6363–6370,
723 doi:10.5194/acp-10-6363-2010, 2010.

724 Chavez, P. S.: An improved dark-object subtraction technique for atmospheric scattering
725 correction of multispectral data, *Remote Sens. Environ.*, 24(3), 459–479,
726 doi:10.1016/0034-4257(88)90019-3, 1988.

727 Cofer III, W. R., Levine, J. S., Winstead, E. L. and Stocks, B. J.: New estimates of nitrous
728 oxide emissions from biomass burning, *Nature*, 349(6311), 689–691 [online] Available
729 from: <http://dx.doi.org/10.1038/349689a0>, 1991.

730 Conny, J. and Slater, J.: Black carbon and organic carbon in aerosol particles from crown
731 fires in the Canadian boreal forest, *J. Geophys. Res.* ... [online] Available from:
732 <http://onlinelibrary.wiley.com/doi/10.1029/2001JD001528/full>, 2002.

733 Daanen, R. P., Ingeman-Nielsen, T., Marchenko, S. S., Romanovsky, V. E., Foged, N.,

734 Stendel, M., Christensen, J. H. and Hornbech Svendsen, K.: Permafrost degradation risk
735 zone assessment using simulation models, *Cryosphere*, 5(4), 1043–1056,
736 doi:10.5194/tc-5-1043-2011, 2011.
737 Dahlback, A. and Stamnes, K.: A new spherical model for computing the radiation field
738 available for photolysis and heating at twilight, *Planet. Space Sci.*, 39(5), 671–683,
739 doi:10.1016/0032-0633(91)90061-E, 1991.
740 Davies, G. M., Gray, A., Rein, G. and Legg, C. J.: Peat consumption and carbon loss due to
741 smouldering wildfire in a temperate peatland, *For. Ecol. Manage.*, 308, 169–177,
742 doi:10.1016/j.foreco.2013.07.051, 2013.
743 Dibb, J. E., Arsenault, M., Peterson, M. C. and Honrath, R. E.: Fast nitrogen oxide
744 photochemistry in Summit, Greenland snow, *Atmos. Environ.*, 36(15–16), 2501–2511,
745 doi:10.1016/S1352-2310(02)00130-9, 2002.
746 Doherty, S. J., Warren, S. G., Grenfell, T. C., Clarke, A. D. and Brandt, R. E.: Light-absorbing
747 impurities in Arctic snow, *Atmos. Chem. Phys.*, 10(23), 11647–11680, doi:10.5194/acp-
748 10-11647-2010, 2010.
749 Drysdale, D.: *An Introduction to Fire Dynamics*, 3rd Editio., John Wiley & Sons, Ltd.,
750 2011.
751 Emde, C., Buras-Schnell, R., Kylling, A., Mayer, B., Gasteiger, J., Hamann, U., Kylling, J.,
752 Richter, B., Pause, C., Dowling, T. and Bugliaro, L.: The libRadtran software package for
753 radiative transfer calculations (version 2.0.1), *Geosci. Model Dev.*, 9(5), 1647–1672,
754 doi:10.5194/gmd-9-1647-2016, 2016.
755 Escuin, S., Navarro, R. and Fernández, P.: Fire severity assessment by using NBR
756 (Normalized Burn Ratio) and NDVI (Normalized Difference Vegetation Index) derived
757 from LANDSAT TM/ETM images, *Int. J. Remote Sens.*, 29(4), 1053–1073,
758 doi:10.1080/01431160701281072, 2008.
759 Evangeliou, N., Balkanski, Y., Cozic, A., Hao, W. M. and Møller, A. P.: Wildfires in
760 Chernobyl-contaminated forests and risks to the population and the environment: A
761 new nuclear disaster about to happen?, *Environ. Int.*, 73, 346–358,
762 doi:10.1016/j.envint.2014.08.012, 2014.
763 Evangeliou, N., Balkanski, Y., Cozic, A., Hao, W. M., Mouillot, F., Thonicke, K., Paugam, R.,
764 Zibtsev, S., Mousseau, T. A., Wang, R., Poulter, B., Petkov, A., Yue, C., Cadule, P., Koffi, B.,
765 Kaiser, J. W., Møller, A. P. and Classen, A. T.: Fire evolution in the radioactive forests of
766 Ukraine and Belarus: Future risks for the population and the environment, *Ecol.*
767 *Monogr.*, 85(1), 49–72, doi:10.1890/14-1227.1, 2015.
768 Evangeliou, N., Zibtsev, S., Myroniuk, V., Zhurba, M., Hamburger, T., Stohl, A., Balkanski,
769 Y., Paugam, R., Mousseau, T. A., Møller, A. P. and Kireev, S. I.: Resuspension and
770 atmospheric transport of radionuclides due to wildfires near the Chernobyl Nuclear
771 Power Plant in 2015: An impact assessment, *Sci. Rep.*, 6, 26062 [online] Available from:
772 <http://www.nature.com/srep/2016/160517/srep26062/full/srep26062.html>, 2016.
773 Fang, X., Thompson, R. L., Saito, T., Yokouchi, Y., Kim, J., Li, S., Kim, K. R., Park, S., Graziosi,
774 F. and Stohl, A.: Sulfur hexafluoride (SF₆) emissions in East Asia determined by inverse
775 modeling, *Atmos. Chem. Phys.*, 14(9), 4779–4791, doi:10.5194/acp-14-4779-2014,
776 2014.
777 Faulkner Burkhart, J., Kylling, A., Schaaf, C. B., Wang, Z., Bogren, W., Storbvold, R., Solbø, S.,
778 Pedersen, C. A. and Gerland, S.: Unmanned aerial system nadir reflectance and MODIS
779 nadir BRDF-adjusted surface reflectances intercompared over Greenland, *Cryosphere*,
780 11(4), 1575–1589, doi:10.5194/tc-11-1575-2017, 2017.
781 Feng, Y., Ramanathan, V. and Kotamarthi, V. R.: Brown carbon: A significant atmospheric
782 absorber of solar radiation, *Atmos. Chem. Phys.*, 13(17), 8607–8621, doi:10.5194/acp-

783 13-8607-2013, 2013.
784 Ferguson, S. A., Collins, R. L., Ruthford, J. and Fukuda, M.: Vertical distribution of
785 nighttime smoke following a wildland biomass fire in boreal Alaska, *J. Geophys. Res.*,
786 108(June), D23, 4743, doi:10.1029/2002JD003324, doi:10.1029/2002JD003324, 2003.
787 Fernandez Anez, N., Garcia Torrent, J., Medic Pejic, L. and Grima Olmedo, C.: Detection of
788 incipient self-ignition process in solid fuels through gas emissions methodology, *J. Loss*
789 *Prev. Process Ind.*, 36, 343–351, doi:10.1016/j.jlp.2015.02.010, 2015.
790 Flanner, M. G., Zender, C. S., Randerson, J. T. and Rasch, P. J.: Present-day climate forcing
791 and response from black carbon in snow, *J. Geophys. Res. Atmos.*, 112(11), 1–17,
792 doi:10.1029/2006JD008003, 2007.
793 Flanner, M. G., Zender, C. S., Hess, P. G., Mahowald, N. M., Painter, T. H., Ramanathan, V.
794 and Rasch, P. J.: Springtime warming and reduced snow cover from carbonaceous
795 particles, *Atmos. Chem. Phys.*, 9, 2481–2497, doi:10.5194/acp-9-2481-2009, 2009.
796 Forster, C., Wandering, U., Wotawa, G., James, P., Mattis, I., Althausen, D., Simmonds, P.,
797 O'Doherty, S., Jennings, S. G., Kleefeld, C., Schneider, J., Trickl, T., Kreipl, S., Jäger, H. and
798 Stohl, A.: Transport of boreal forest fire emissions from Canada to Europe, *J. Geophys.*
799 *Res.*, 106, 22887, doi:10.1029/2001JD900115, 2001.
800 Forster, C., Stohl, A. and Seibert, P.: Parameterization of convective transport in a
801 Lagrangian particle dispersion model and its evaluation, *J. Appl. Meteorol. Climatol.*,
802 46(4), 403–422, doi:10.1175/JAM2470.1, 2007.
803 Freitas, S. R., Longo, K. M., Chatfield, R., Latham, D., Silva Dias, M. a. F., Andreae, M. O.,
804 Prins, E., Santos, J. C., Gielow, R. and Carvalho, J. a.: Including the sub-grid scale plume
805 rise of vegetation fires in low resolution atmospheric transport models, *Atmos. Chem.*
806 *Phys. Discuss.*, 6(6), 11521–11559, doi:10.5194/acpd-6-11521-2006, 2006.
807 Freitas, S. R., Longo, K. M., Trentmann, J. and Latham, D.: Technical Note: Sensitivity of 1-
808 D smoke plume rise models to the inclusion of environmental wind drag, *Atmos. Chem.*
809 *Phys.*, 10(2), 585–594, doi:10.5194/acp-10-585-2010, 2010.
810 French, N., Kasischke, E., Hall, R., Murphy, K., Verbyla, D., Hoy, E. and Allen, J.: Using
811 Landsat data to assess fire and burn severity in the North American boreal forest region:
812 an overview and summary of results, *Int. J. Wildl. Fire*, 17(4), 443–462,
813 doi:10.1071/WF08007, 2008.
814 Fromm, M., Bevilacqua, R., Servranckx, R., Rosen, J., Thayer, J. P., Herman, J. and Larko, D.:
815 Pyro-cumulonimbus injection of smoke to the stratosphere: Observations and impact of
816 a super blowup in northwestern Canada on 3-4 August 1998, *J. Geophys. Res. D Atmos.*,
817 110(8), 1–17, doi:10.1029/2004JD005350, 2005.
818 Giglio, L., Desclotres, J., Justice, C. O. and Kaufman, Y. J.: An enhanced contextual fire
819 detection algorithm for MODIS, *Remote Sens. Environ.*, 87(2–3), 273–282,
820 doi:10.1016/S0034-4257(03)00184-6, 2003.
821 Grannas, A. M., Shepson, P. B. and Filley, T. R.: Photochemistry and nature of organic
822 matter in Arctic and Antarctic snow, *Global Biogeochem. Cycles*, 18(1), n/a-n/a,
823 doi:10.1029/2003GB002133, 2004.
824 Grythe, H., Kristiansen, N. I., Groot Zwaaftink, C. D., Eckhardt, S., Ström, J., Tunved, P.,
825 Krejci, R. and Stohl, A.: A new aerosol wet removal scheme for the Lagrangian particle
826 model FLEXPARTv10, *Geosci. Model Dev.*, 10, 1447–1466, doi:10.5194/gmd-10-1447-
827 2017, 2017.
828 Hansen, J. and Nazarenko, L.: Soot climate forcing via snow and ice albedos, *Proc. Natl.*
829 *Acad. Sci. U. S. A.*, 101(2), 423–428, doi:10.1073/pnas.2237157100, 2004.
830 Hansen, J., Sato, M., Ruedy, R., Nazarenko, L., Lacis, A., Schmidt, G. A., Russell, G., Aleinov,
831 I., Bauer, M., Bauer, S., Bell, N., Cairns, B., Canuto, V., Chandler, M., Cheng, Y., Del Genio, A.,

832 Faluvegi, G., Fleming, E., Friend, A., Hall, T., Jackman, C., Kelley, M., Kiang, N., Koch, D.,
833 Lean, J., Lerner, J., Lo, K., Menon, S., Miller, R., Minnis, P., Novakov, T., Oinas, V., Perlwitz,
834 J., Perlwitz, J., Rind, D., Romanou, A., Shindell, D., Stone, P., Sun, S., Tausnev, N., Thresher,
835 D., Wielicki, B., Wong, T., Yao, M. and Zhang, S.: Efficacy of climate forcings, *J. Geophys.*
836 *Res. D Atmos.*, 110(18), 1–45, doi:10.1029/2005JD005776, 2005.

837 Hao, W. M. and Ward, D. E.: Methane production from global biomass burning, *J.*
838 *Geophys. Res. Atmos.*, 98(D11), 20657–20661, doi:10.1029/93JD01908, 1993.

839 Hao, W. M., Petkov, A., Nordgren, B. L., Silverstein, R. P., Corley, R. E., Urbanski, S. P.,
840 Evangeliou, N., Balkanski, Y. and Kinder, B.: Daily black carbon emissions from fires in
841 Northern Eurasia from 2002 to 2013, *Geosci. Model Dev.*, 9, 4461–4474,
842 doi:10.5194/gmd-9-4461-2016, 2016.

843 Holben, B. N.: Characteristics of maximum-value composite images from temporal
844 AVHRR data, *Int. J. Remote Sens.*, 7(11), 1417–1434, doi:10.1080/01431168608948945,
845 1986.

846 Holben, B. N., Eck, T. F., Slutsker, I., Tanré, D., Buis, J. P., Setzer, A., Vermote, E., Reagan, J.
847 A., Kaufman, Y. J., Nakajima, T., Lavenu, F., Jankowiak, I. and Smirnov, A.: AERONET—A
848 Federated Instrument Network and Data Archive for Aerosol Characterization, *Remote*
849 *Sens. Environ.*, 66(1), 1–16, doi:10.1016/S0034-4257(98)00031-5, 1998.

850 Hosseini, S., Li, Q., Cocker, D., Weise, D., Miller, A., Shrivastava, M., Miller, J. W.,
851 Mahalingam, S., Princevac, M. and Jung, H.: Particle size distributions from laboratory-
852 scale biomass fires using fast response instruments, *Atmos. Chem. Phys.*, 10(16), 8065–
853 8076, doi:10.5194/acp-10-8065-2010, 2010.

854 Hu, Y., Fernandez-Anez, N., Smith, T. E. L. and Rein, G.: Review of emissions from
855 smouldering peat fires and their contribution to regional haze episodes, *Int. J. Wildl.*
856 *Fire*, 27(5), 293–312, doi:10.1071/WF17084, 2018.

857 IPCC: Climate Change 2013: The Physical Science Basis. Contribution to the Fifth
858 Assessment Report of the Intergovernmental Panel on Climate Change., edited by T. F.
859 Stocker, D. Qin, G.-K. Plattner, M. M. B. Tignor, S. K. Allen, J. Boschung, A. Nauels, Y. Xia, V.
860 Bex, and P. M. Midgley, Cambridge University Press., 2013.

861 Jacobson, M. Z.: Strong radiative heating due to the mixing state of black carbon in
862 atmospheric aerosols, *Nature*, 409(6821), 695–697, doi:10.1038/35055518, 2001.

863 Jedrzejek, B., Drees, B., Daniëls, F. J. A. and Hölzel, N.: Vegetation pattern of mountains in
864 West Greenland - a baseline for long-term surveillance of global warming impacts, *Plant*
865 *Ecol. Divers.*, 6(3–4), 405–422, doi:10.1080/17550874.2013.802049, 2013.

866 Jo, D. S., Park, R. J., Lee, S., Kim, S. W. and Zhang, X.: A global simulation of brown carbon:
867 Implications for photochemistry and direct radiative effect, *Atmos. Chem. Phys.*, 16(5),
868 3413–3432, doi:10.5194/acp-16-3413-2016, 2016.

869 Justice, C. O., Giglio, L., Korontzi, S., Owens, J., Morisette, J. T., Roy, D., Descloitres, J.,
870 Alleaume, S., Petitcolin, F. and Kaufman, Y.: The MODIS fire products, *Remote Sens.*
871 *Environ.*, 83(1–2), 244–262, doi:10.1016/S0034-4257(02)00076-7, 2002.

872 Kaiser, J. W., Heil, A., Andreae, M. O., Benedetti, A., Chubarova, N., Jones, L., Morcrette, J. J.,
873 Razinger, M., Schultz, M. G., Suttie, M. and Van Der Werf, G. R.: Biomass burning
874 emissions estimated with a global fire assimilation system based on observed fire
875 radiative power, *Biogeosciences*, 9(1), 527–554, doi:10.5194/bg-9-527-2012, 2012.

876 Kato, S., Ackerman, T. P., Mather, J. H. and Clothiaux, E. E.: The k-distribution method and
877 correlated-k approximation for a shortwave radiative transfer model, *J. Quant.*
878 *Spectrosc. Radiat. Transf.*, 62(1), 109–121, doi:10.1016/S0022-4073(98)00075-2, 1999.

879 Keegan, K. M., Albert, M. R., McConnell, J. R. and Baker, I.: Climate change and forest fires
880 synergistically drive widespread melt events of the Greenland Ice Sheet, , 1–4,

881 doi:10.1073/pnas.1405397111, 2014.
882 Key, C. H. and Benson, N. C.: Landscape assessment: Sampling and analysis methods,
883 USDA For. Serv. Gen. Tech. Rep. RMRS-GTR-164-CD, (June), 1–55,
884 doi:10.1002/app.1994.070541203, 2006.
885 Klimont, Z., Kupiainen, K., Heyes, C., Purohit, P., Cofala, J., Rafaj, P., Borken-Kleefeld, J. and
886 Schöpp, W.: Global anthropogenic emissions of particulate matter including black
887 carbon, *Atmos. Chem. Phys.*, 17, 8681–8723, doi:10.5194/acp-17- 50 8681-2017, 2017.
888 Lavoie, C. and Pellerin, S.: Fires in temperate peatlands (southern Quebec): past and
889 recent trends, *Can. J. Bot.*, 85(3), 263–272, doi:10.1139/B07-012, 2007.
890 Legrand, M., Preunkert, S., Jourdain, B., Guilhermet, J., Faïn, X., Alekhina, I. and Petit, J. R.:
891 Water-soluble organic carbon in snow and ice deposited at Alpine, Greenland, and
892 Antarctic sites: A critical review of available data and their atmospheric relevance, *Clim.*
893 *Past*, 9(5), 2195–2211, doi:10.5194/cp-9-2195-2013, 2013.
894 Legrand, M., McConnell, J., Fischer, H., Wolff, E. W., Preunkert, S., Arienzo, M., Chellman,
895 N., Leuenberger, D., Maselli, O., Place, P., Sigl, M., Schiöpbach, S. and Flannigan, M.:
896 Boreal fire records in Northern Hemisphere ice cores: A review, *Clim. Past*, 12(10),
897 2033–2059, doi:10.5194/cp-12-2033-2016, 2016.
898 Leino, K., Riuttanen, L., Nieminen, T., Väänänen, R., Pohja, T., Keronen, P., Järvi, L., Aalto,
899 P. P., Virkkula, A., Kerminen, V. M., Petäjä, T., Kulmala, M., Nieminen, T., Dal Maso, M. and
900 Virkkula, A.: Biomass-burning smoke episodes in Finland from eastern European
901 wildfires, *Boreal Environ. Res.*, 19(x), 275–292, 2014.
902 Lelieveld, J., Evans, J. S., Fnais, M., Giannadaki, D. and Pozzer, A.: The contribution of
903 outdoor air pollution sources to premature mortality on a global scale., *Nature*,
904 525(7569), 367–71, doi:10.1038/nature15371, 2015.
905 Leung, F. Y. T., Logan, J. A., Park, R., Hyer, E., Kasischke, E., Streets, D. and Yurganov, L.:
906 Impacts of enhanced biomass burning in the boreal forests in 1998 on tropospheric
907 chemistry and the sensitivity of model results to the injection height of emissions, *J.*
908 *Geophys. Res. Atmos.*, 112(10), 1–15, doi:10.1029/2006JD008132, 2007.
909 Lim, H. J., Turpin, B. J., Russell, L. M. and Bates, T. S.: Organic and elemental carbon
910 measurements during ACE-Asia suggest a longer atmospheric lifetime for elemental
911 carbon, *Environ. Sci. Technol.*, 37(14), 3055–3061, doi:10.1021/es020988s, 2003.
912 Limbeck, A., Kulmala, M. and Puxbaum, H.: Secondary organic aerosol formation in the
913 atmosphere via heterogeneous reaction of gaseous isoprene on acidic particles,
914 *Geophys. Res. Lett.*, 30(19), 4–7, doi:10.1029/2003GL017738, 2003.
915 Long, C. M., Nascarella, M. A. and Valberg, P. A.: Carbon black vs. black carbon and other
916 airborne materials containing elemental carbon: Physical and chemical distinctions,
917 *Environ. Pollut.*, 181, 271–286, doi:10.1016/j.envpol.2013.06.009, 2013.
918 Lyons, W. B., Welch, K. A. and Doggett, J. K.: Organic carbon in Antarctic snow, *Geophys.*
919 *Res. Lett.*, 34(2), 2–5, doi:10.1029/2006GL028150, 2007.
920 Magnan, G., Lavoie, M. and Payette, S.: Impact of fire on long-term vegetation dynamics
921 of ombrotrophic peatlands in northwestern Québec, Canada, *Quat. Res.*, 77(1), 110–121,
922 doi:http://dx.doi.org/10.1016/j.yqres.2011.10.006, 2012.
923 Massling, A., Nielsen, I. E., Kristensen, D., Christensen, J. H., Sorensen, L. L., Jensen, B.,
924 Nguyen, Q. T., Nøjgaard, J. K., Glasius, M. and Skov, H.: Atmospheric black carbon and
925 sulfate concentrations in Northeast Greenland, *Atmos. Chem. Phys.*, 15(16), 9681–9692,
926 doi:10.5194/acp-15-9681-2015, 2015.
927 Mayer, B. and Kylling, A.: Technical note: The libRadtran software package for radiative
928 transfer calculations - description and examples of use, *Atmos. Chem. Phys.*, 5(7), 1855–
929 1877, doi:10.5194/acp-5-1855-2005, 2005.

930 Mukai, H. and Ambe, Y.: Characterization of a humic acid-like brown substance in
931 airborne particulate matter and tentative identification of its origin, *Atmos. Environ.*,
932 20(5), 813–819, doi:[https://doi.org/10.1016/0004-6981\(86\)90265-9](https://doi.org/10.1016/0004-6981(86)90265-9), 1986.
933 Myhre, G., Shindell, D., Bréon, F.-M., Collins, W., Fuglestedt, J., Huang, J., Koch, D.,
934 Lamarque, J.-F., Lee, D., Mendoza, B., Nakajima, T., Robock, A., Stephens, G., Takemura, T.
935 and Zhang, H.: Anthropogenic and Natural Radiative Forcing, in *Climate Change 2013:*
936 *The Physical Science Basis. Contribution of Working Group I to the Fifth Assessment*
937 *Report of the Intergovernmental Panel on Climate Change*, edited by Stocker, T.F., D. Qin,
938 G.-K. Plattner, M. Tignor, S. K. Allen, J. Boschung, A. Nauels, Y. Xia, V. Bex, and P. M.
939 Midgley, pp. 659–740, Cambridge University Press, Cambridge, United Kingdom and
940 New York, NY, USA., 2013.
941 NASA: FIRMS. Web Fire Mapper, [online] Available from:
942 <https://firms.modaps.eosdis.nasa.gov/firemap/> (Accessed 5 September 2017a), 2017.
943 NASA: Roundtable: The Greenland Wildfire, [online] Available from:
944 [https://earthobservatory.nasa.gov/blogs/earthmatters/2017/08/10/roundtable-the-](https://earthobservatory.nasa.gov/blogs/earthmatters/2017/08/10/roundtable-the-greenland-wildfire/)
945 [greenland-wildfire/](https://earthobservatory.nasa.gov/blogs/earthmatters/2017/08/10/roundtable-the-greenland-wildfire/) (Accessed 6 September 2017b), 2017.
946 NASA: Wildfires Continue to Beleaguer Western Canada, [online] Available from:
947 [https://www.nasa.gov/image-feature/goddard/2017/wildfires-continue-to-beleaguer-](https://www.nasa.gov/image-feature/goddard/2017/wildfires-continue-to-beleaguer-western-canada)
948 [western-canada](https://www.nasa.gov/image-feature/goddard/2017/wildfires-continue-to-beleaguer-western-canada) (Accessed 29 October 2017c), 2017.
949 New Scientist Magazine: Largest ever wildfire in Greenland seen burning from space,
950 [online] Available from: [https://www.newscientist.com/article/2143159-largest-ever-](https://www.newscientist.com/article/2143159-largest-ever-wildfire-in-greenland-seen-burning-from-space/)
951 [wildfire-in-greenland-seen-burning-from-space/](https://www.newscientist.com/article/2143159-largest-ever-wildfire-in-greenland-seen-burning-from-space/) (Accessed 6 September 2017), 2017.
952 Page, S. E., Siegert, F., Rieley, J. O., Boehm, H.-D. V., Jada, A. and Limin, S.: The amount of
953 carbon released from peat and forest fires in Indonesia during 1997, *Nature*, 420(19),
954 61–65, doi:10.1038/nature01131, 2015.
955 Paugam, R., Wooster, M. and Atherton, J.: Development and optimization of a wildfire
956 plume rise model based on remote sensing data inputs – Part 2, , doi:10.5194/acpd-15-
957 9815-2015, 2015.
958 Pokhrel, R. P., Wagner, N. L., Langridge, J. M., Lack, D. A., Jayarathne, T., Stone, E. A.,
959 Stockwell, C. E., Yokelson, R. J. and Murphy, S. M.: Parameterization of single-scattering
960 albedo (SSA) and absorption Ångström exponent (AAE) with EC/OC for aerosol
961 emissions from biomass burning, *Atmos. Chem. Phys.*, 16(15), 9549–9561,
962 doi:10.5194/acp-16-9549-2016, 2016.
963 Polashenski, C. M., Dibb, J. E., Flanner, M. G., Chen, J. Y., Courville, Z. R., Lai, A. M., Schauer,
964 J. J., Shafer, M. M. and Bergin, M.: Neither dust nor black carbon causing apparent albedo
965 decline in Greenland’s dry snow zone: Implications for MODIS C5 surface reflectance,
966 *Geophys. Res. Lett.*, 42(21), 9319–9327, doi:10.1002/2015GL065912, 2015.
967 Randerson, J. T., Chen, Y., Van Der Werf, G. R., Rogers, B. M. and Morton, D. C.: Global
968 burned area and biomass burning emissions from small fires, *J. Geophys. Res.*
969 *Biogeosciences*, 117(4), doi:10.1029/2012JG002128, 2012.
970 Reddy, A. D., Hawbaker, T. J., Wurster, F., Zhu, Z., Ward, S., Newcomb, D. and Murray, R.:
971 Quantifying soil carbon loss and uncertainty from a peatland wildfire using multi-
972 temporal LiDAR, *Remote Sens. Environ.*, 170, 306–316, doi:10.1016/j.rse.2015.09.017,
973 2015.
974 Rémy, S., Veira, A., Paugam, R., Sofiev, M., Kaiser, J. W., Marenco, F., Burton, S. P.,
975 Benedetti, A., Engelen, R. J., Ferrare, R. and Hair, J. W.: Two global data sets of daily fire
976 emission injection heights since 2003, , 2921–2942, doi:10.5194/acp-17-2921-2017,
977 2017.
978 Restuccia, F., Ptak, N. and Rein, G.: Self-heating behavior and ignition of shale rock,

979 Combust. Flame, 176, 213–219, doi:10.1016/j.combustflame.2016.09.025, 2017a.
980 Restuccia, F., Huang, X. and Rein, G.: Self-ignition of natural fuels: Can wildfires of
981 carbon-rich soil start by self-heating?, Fire Saf. J., 91(February), 828–834,
982 doi:10.1016/j.firesaf.2017.03.052, 2017b.
983 von Schneidemesser, E., Schauer, J. J., Hagler, G. S. W. and Bergin, M. H.: Concentrations
984 and sources of carbonaceous aerosol in the atmosphere of Summit, Greenland, Atmos.
985 Environ., 43(27), 4155–4162, doi:10.1016/j.atmosenv.2009.05.043, 2009.
986 Seiler, W. and Crutzen, P. J.: Estimates of gross and net fluxes of carbon between the
987 biosphere and the atmosphere from biomass burning, Clim. Change, 2(3), 207–247,
988 doi:10.1007/BF00137988, 1980.
989 SERMITSIAQ: Se billeder: Naturbrand udvikler kraftig røg, , in Danish [online] Available
990 from: <http://sermitsiaq.ag/se-billeder-naturbrand-udvikler-kraftig-roeg> (Accessed 6
991 September 2017), 2017.
992 Shetler, G., Turetsky, M. R., Kane, E. and Kasischke, E.: Sphagnum mosses limit total
993 carbon consumption during fire in Alaskan black spruce forests, Can. J. For. Res., 38(8),
994 2328–2336, doi:10.1139/X08-057, 2008.
995 Shi, Y., Matsunaga, T., Saito, M., Yamaguchi, Y. and Chen, X.: Comparison of global
996 inventories of CO₂ emissions from biomass burning during 2002–2011 derived from
997 multiple satellite products, Environ. Pollut., 206, 479–487,
998 doi:10.1016/j.envpol.2015.08.009, 2015.
999 Skeie, R. B., Berntsen, T., Myhre, G., Pedersen, C. A., Strām, J., Gerland, S. and Ogren, J. A.:
1000 Black carbon in the atmosphere and snow, from pre-industrial times until present,
1001 Atmos. Chem. Phys., 11(14), 6809–6836, doi:10.5194/acp-11-6809-2011, 2011.
1002 Smirnov, N. S., Korotkov, V. N. and Romanovskaya, A. A.: Black carbon emissions from
1003 wildfires on forest lands of the Russian Federation in 2007–2012, Russ. Meteorol.
1004 Hydrol., 40(7), 435–442, doi:10.3103/S1068373915070018, 2015.
1005 Stamnes, K., Tsay, S.-C., Wiscombe, W. and Jayaweera, K.: Numerically stable algorithm
1006 for discrete-ordinate-method radiative transfer in multiple scattering and emitting
1007 layered media, Appl. Opt., 27(12), 2502, doi:10.1364/AO.27.002502, 1988.
1008 Stendel, M., Christensen, J. H. and Petersen, D.: Arctic Climate and Climate Change with a
1009 Focus on Greenland, Adv. Ecol. Res., 40(07), 13–43, doi:10.1016/S0065-
1010 2504(07)00002-5, 2008.
1011 Stockwell, C. E., Jayarathne, T., Cochrane, M. A., Ryan, K. C., Putra, E. I., Saharjo, B. H.,
1012 Nurhayati, A. D., Albar, I., Blake, D. R., Simpson, I. J., Stone, E. A. and Yokelson, R. J.: Field
1013 measurements of trace gases and aerosols emitted by peat fires in Central Kalimantan,
1014 Indonesia, during the 2015 El Niño, Atmos. Chem. Phys., 16(18), 11711–11732,
1015 doi:10.5194/acp-16-11711-2016, 2016.
1016 Stohl, A., Forster, C., Frank, A., Seibert, P. and Wotawa, G.: Technical note: The Lagrangian
1017 particle dispersion model FLEXPART version 6.2, Atmos. Chem. Phys., 5(9), 2461–2474,
1018 doi:10.5194/acp-5-2461-2005, 2005.
1019 Stohl, A., Andrews, E., Burkhart, J. F., Forster, C., Herber, A., Hoch, S. W., Kowal, D.,
1020 Lunder, C., Mefford, T., Ogren, J. A., Sharma, S., Spichtinger, N., Stebel, K., Stone, R., Ström,
1021 J., Tørseth, K., Wehrli, C. and Yttri, K. E.: Pan-Arctic enhancements of light absorbing
1022 aerosol concentrations due to North American boreal forest fires during summer 2004, J.
1023 Geophys. Res. Atmos., 111(22), 1–20, doi:10.1029/2006JD007216, 2006.
1024 Stohl, A., Berg, T., Burkhart, J. F., Fjærraa, A. M., Forster, C., Herber, A., Hov, Ø., Lunder, C.,
1025 McMillan, W. W., Oltmans, S., Shiobara, M., Simpson, D., Solberg, S., Stebel, K., Ström, J.,
1026 Tørseth, K., Treffeisen, R., Virkkunen, K. and Yttri, K. E.: Arctic smoke & record
1027 high air pollution levels in the European Arctic due to agricultural fires in Eastern

1028 Europe in spring 2006, *Atmos. Chem. Phys.*, 7(2), 511–534, doi:10.5194/acp-7-511-
1029 2007, 2007.

1030 Stohl, A., Prata, A. J., Eckhardt, S., Clarisse, L., Durant, A., Henne, S., Kristiansen, N. I.,
1031 Minikin, A., Schumann, U., Seibert, P., Stebel, K., Thomas, H. E., Thorsteinsson, T., Tørseth,
1032 K. and Weinzierl, B.: Determination of time-and height-resolved volcanic ash emissions
1033 and their use for quantitative ash dispersion modeling: The 2010 Eyjafjallajökull
1034 eruption, *Atmos. Chem. Phys.*, 11(9), 4333–4351, doi:10.5194/acp-11-4333-2011, 2011.

1035 Stohl, A., Klimont, Z., Eckhardt, S., Kupiainen, K., Shevchenko, V. P., Kopeikin, V. M. and
1036 Novigatsky, A. N.: Black carbon in the Arctic: The underestimated role of gas flaring and
1037 residential combustion emissions, *Atmos. Chem. Phys.*, 13(17), 8833–8855,
1038 doi:10.5194/acp-13-8833-2013, 2013.

1039 Stroeve, J., Box, J. E., Gao, F., Liang, S., Nolin, A. and Schaaf, C.: Accuracy assessment of the
1040 MODIS 16-day albedo product for snow: Comparisons with Greenland in situ
1041 measurements, *Remote Sens. Environ.*, 94(1), 46–60, doi:10.1016/j.rse.2004.09.001,
1042 2005.

1043 Sunderman, S. O. and Weisberg, P. J.: Remote sensing approaches for reconstructing fire
1044 perimeters and burn severity mosaics in desert spring ecosystems, *Remote Sens.*
1045 *Environ.*, 115(9), 2384–2389, doi:10.1016/j.rse.2011.05.001, 2011.

1046 Turetsky, M. R., Donahue, W. F. and Benscoter, B. W.: Experimental drying intensifies
1047 burning and carbon losses in a northern peatland, *Nat. Commun.*, 2, 514,
1048 doi:10.1038/ncomms1523, 2011.

1049 Turetsky, M. R., Benscoter, B., Page, S., Rein, G., van der Werf, G. R. and Watts, A.: Global
1050 vulnerability of peatlands to fire and carbon loss, *Nat. Geosci.*, 8(1), 11–14,
1051 doi:10.1038/ngeo2325, 2014.

1052 Urbanski, S. P., Hao, W. M. and Nordgren, B.: The wildland fire emission inventory:
1053 Western United States emission estimates and an evaluation of uncertainty, *Atmos.*
1054 *Chem. Phys.*, 11(24), 12973–13000, doi:10.5194/acp-11-12973-2011, 2011.

1055 Wandji Nyamsi, W., Arola, A., Blanc, P., Lindfors, a. V., Cesnulyte, V., Pitkänen, M. R. a. and
1056 Wald, L.: Technical Note: A novel parameterization of the transmissivity due to ozone
1057 absorption in the distribution method and correlated approximation of Kato et al.
1058 (1999) over the UV band, *Atmos. Chem. Phys.*, 15(13), 7449–7456, doi:10.5194/acp-15-
1059 7449-2015, 2015.

1060 Warren, S. G.: Can black carbon in snow be detected by remote sensing?, *J. Geophys. Res.*
1061 *Atmos.*, 118(2), 779–786, doi:10.1029/2012JD018476, 2013.

1062 Wieder, R. K., Scott, K. D., Kamminga, K., Vile, M. A., Vitt, D. H., Bone, T., Xu, B., Benscoter,
1063 B. W. and Bhatti, J. S.: Postfire carbon balance in boreal bogs of Alberta, Canada, *Glob.*
1064 *Chang. Biol.*, 15(1), 63–81, doi:10.1111/j.1365-2486.2008.01756.x, 2009.

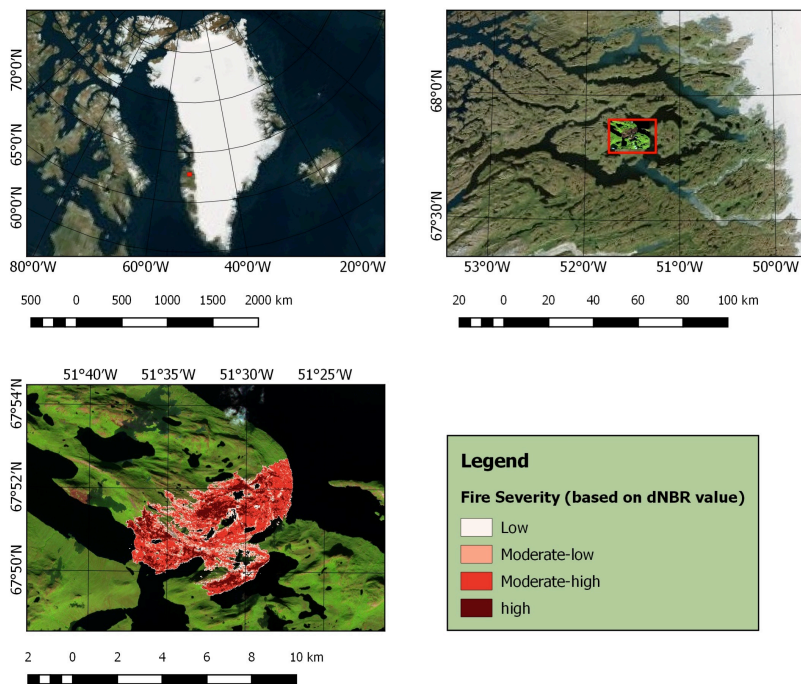
1065 Winiger, P., Andersson, A., Eckhardt, S., Stohl, A., Semiletov, I. P., Dudarev, O. V., Charkin,
1066 A., Shakhova, N., Klimont, Z., Heyes, C. and Gustafsson, Ö.: Siberian Arctic black carbon
1067 sources constrained by model and observation, *Proc. Natl. Acad. Sci.*, 114(7), E1054–
1068 E1061, doi:10.1073/pnas.1613401114, 2017.

1069 Winker, D. M., Vaughan, M. A., Omar, A., Hu, Y., Powell, K. A., Liu, Z., Hunt, W. H. and
1070 Young, S. A.: Overview of the CALIPSO mission and CALIOP data processing algorithms, *J.*
1071 *Atmos. Ocean. Technol.*, 26(11), 2310–2323, doi:10.1175/2009JTECHA1281.1, 2009.

1072 Wu, D., Huang, X., Norman, F., Verplaetsen, F., Berghmans, J. and Van Den Bulck, E.:
1073 Experimental investigation on the self-ignition behaviour of coal dust accumulations in
1074 oxy-fuel combustion system, *Fuel*, 160, 245–254, doi:10.1016/j.fuel.2015.07.050, 2015.

1075 Wu, G. M., Cong, Z. Y., Kang, S. C., Kawamura, K., Fu, P. Q., Zhang, Y. L., Wan, X., Gao, S. P.
1076 and Liu, B.: Brown carbon in the cryosphere: Current knowledge and perspective, *Adv.*

1077 Clim. Chang. Res., 7(1-2), 82-89, doi:10.1016/j.accre.2016.06.002, 2016.
1078 Zhuravleva, T. B., Kabanov, D. M., Nasrtdinov, I. M., Russkova, T. V., Sakerin, S. M.,
1079 Smirnov, A. and Holben, B. N.: Radiative characteristics of aerosol during extreme fire
1080 event over Siberia in summer 2012, Atmos. Meas. Tech., 10(1), 179-198,
1081 doi:10.5194/amt-10-179-2017, 2017.
1082
1083

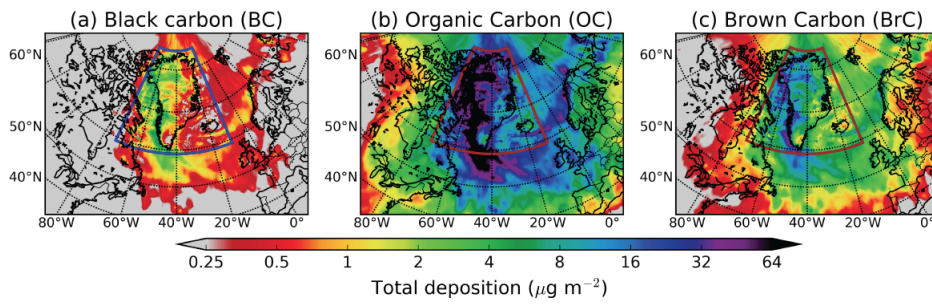


1085
 1086 **Figure 1.** Map of Greenland (upper left) and zoomed map marked with fire location (upper
 1087 right and burned area classification (bottom) in terms of fire severity according to Sentinel 2A
 1088 images for fires burning in Greenland in August 2017. To delineate fire perimeters, both
 1089 Landsat 8 OLI and Sentinel 1A – 2A data were used (Table 1).

1090

Nikolaos Evangeliou 22/12/2018 08:33
 Deleted: Table 1

CUMULATIVE DEPOSITION (31 August 2017)

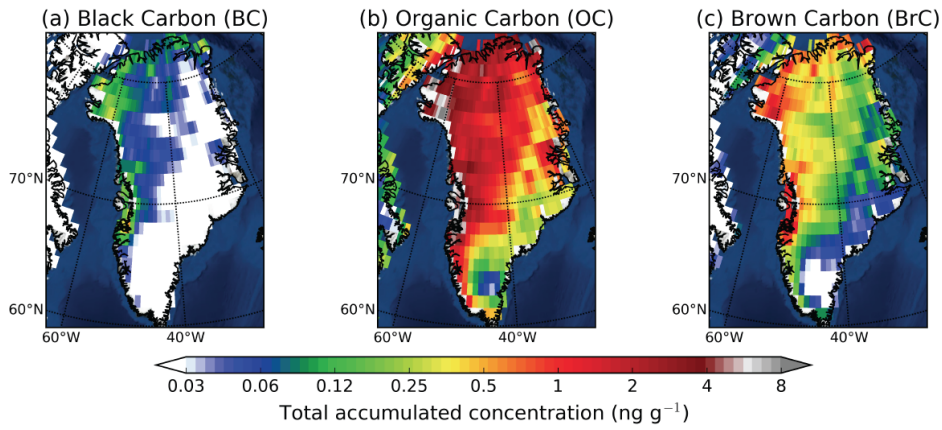


1092

1093 **Figure 2.** Total (wet and dry) deposition of (a) BC, (b) OC and (c) BrC (in $\mu\text{g m}^{-2}$) from the
1094 Greenland fires until 31 August 2017. The colored rectangle depicts the nested high-
1095 resolution domain.

1096

SNOW CONCENTRATIONS BASED ON SNOW ACCUMULATION FROM ECMWF

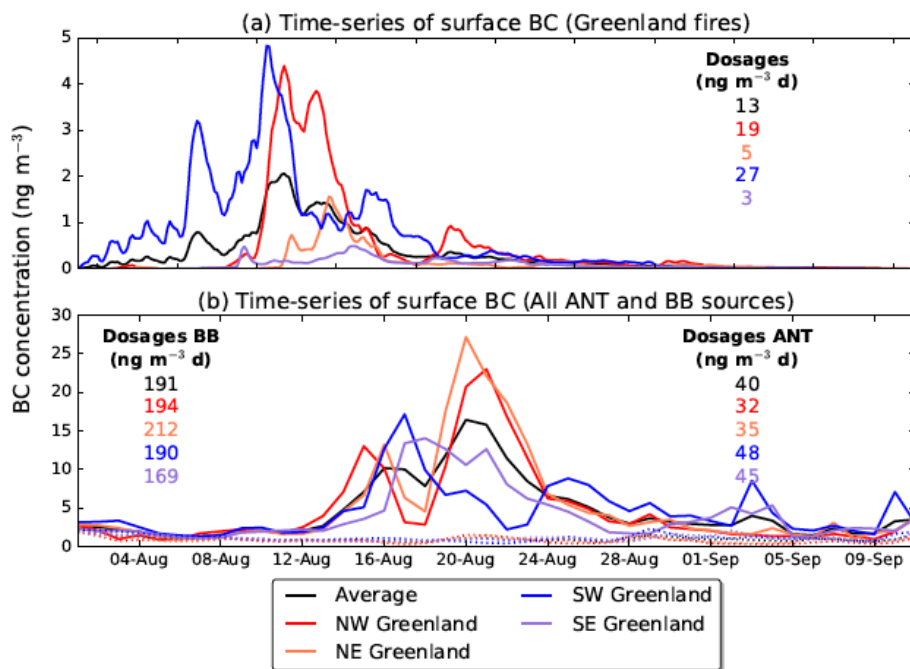


1097

1098 **Figure 3.** Calculated snow concentrations of (a) BC, (b) OC and (c) BrC over Greenland
1099 based on the modeled deposition and the snow precipitation (large scale and convective)
1100 adopted from the operational ECMWF data that were used in our simulation (see section 2.3).

1101

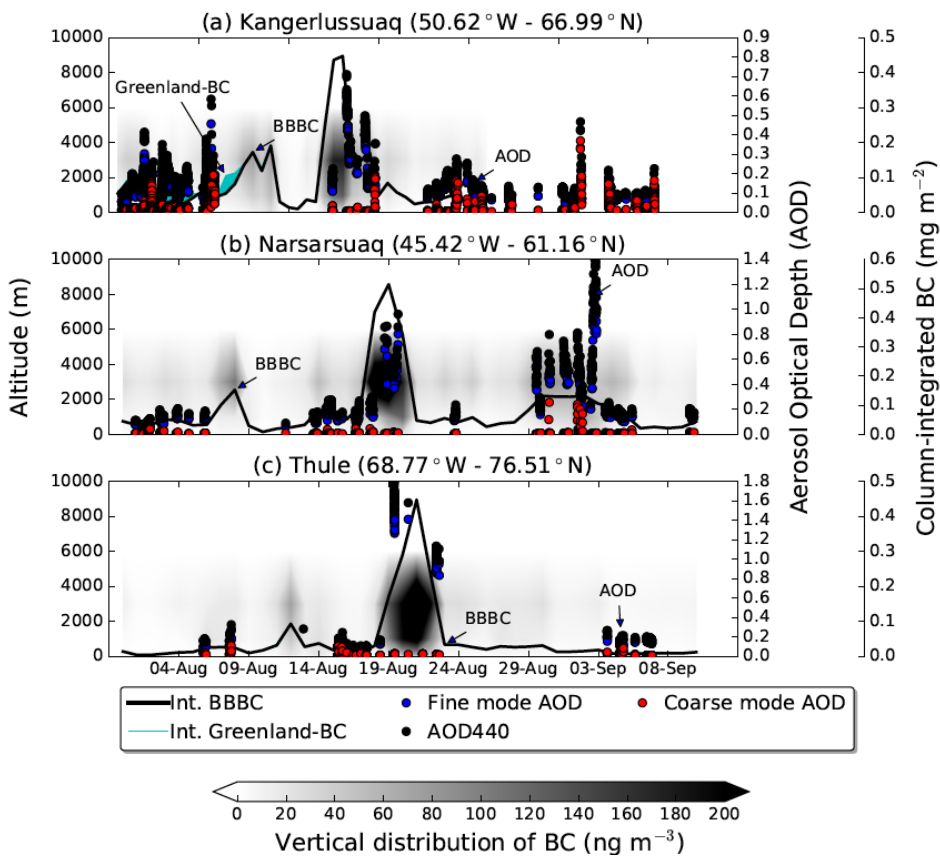
1102



1103

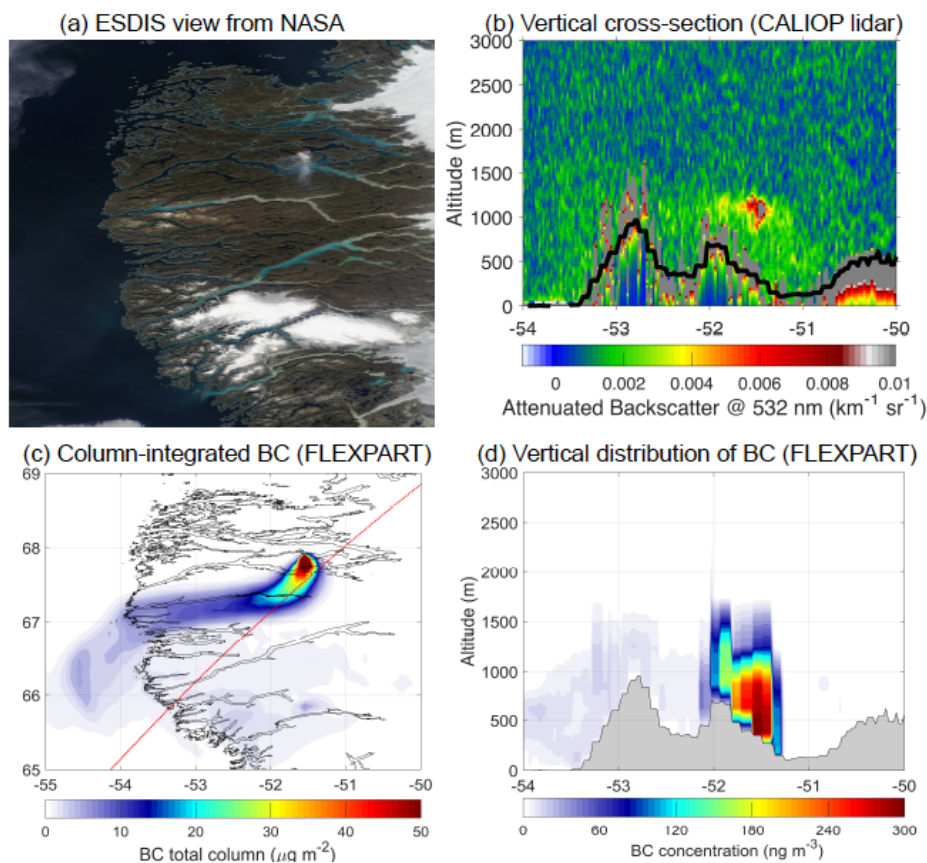
1104 **Figure 4.** (a) Time-series of surface BC concentrations in Northwestern, Northeastern,
1105 Southwestern and Southeastern Greenland from the summer 2017 fires in Western Greenland.
1106 (b) Time-series of surface BC concentrations in Northwestern, Northeastern, Southwestern
1107 and Southeastern Greenland from global anthropogenic (ANT, dashed lines) and biomass
1108 burning (BB, solid lines) emissions for the same period. The numbers represent the respective
1109 dosages (time-integrated concentrations) for the time period shown. The color codes are
1110 reported in the legend.

1111



1112
 1113 **Figure 5.** Contour plot of the vertical distribution of simulated BC (altitude a.g.l. shown on
 1114 left y-axis) as a function of time (x-axis) and time-series of column-integrated simulated BC
 1115 (extended right axis) from fires burning outside Greenland (black line) and Greenland fires
 1116 (cyan stacked area). Column-integrated BC from anthropogenic sources was extremely small
 1117 and it is not plotted here. Time-series for fine mode (blue) and coarse (red) AOD at 500 nm
 1118 and total AOD at 400 nm (black) correspond to the right y-axis. The three panels show results
 1119 for stations (a) Kangerlussuaq, (b) Narsarsuaq and (c) Thule (sorted from the closest to the
 1120 farthest station).

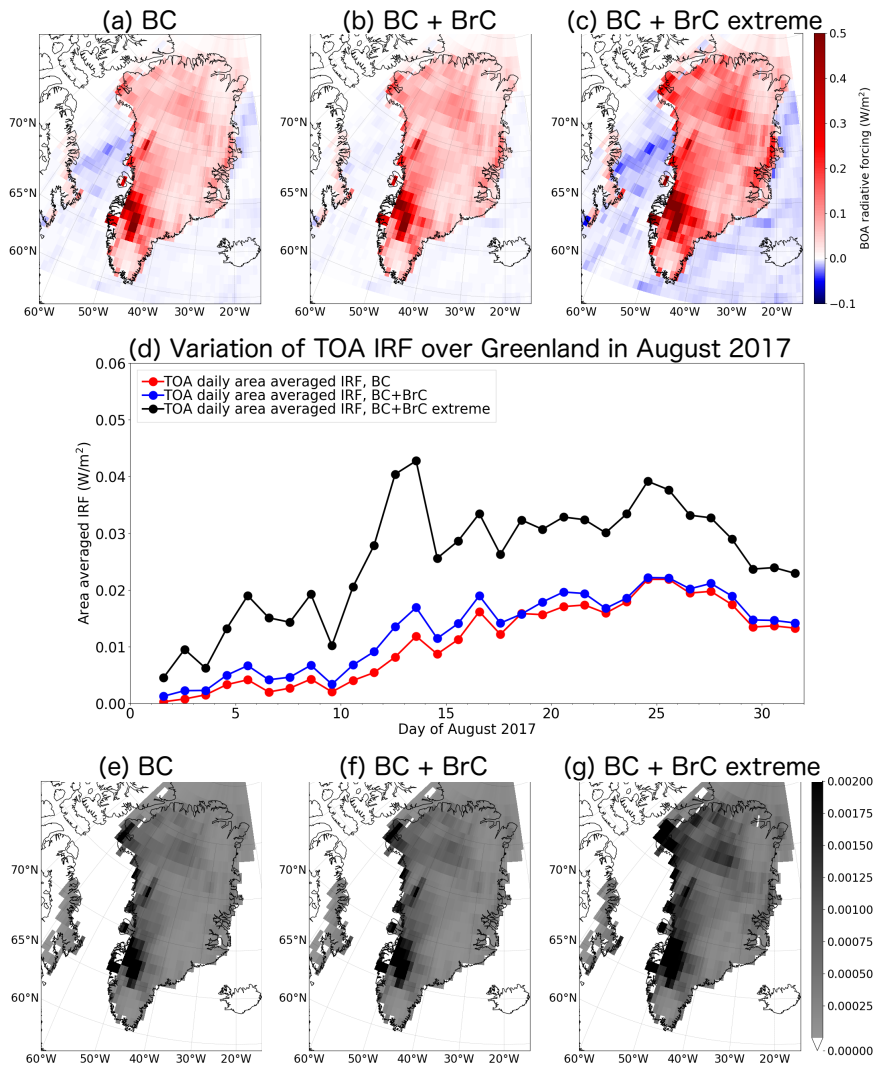
1121



1123

1124 **Figure 6.** (a) Worldview application from the NASA/Goddard Space Flight Center Earth
 1125 Science Data and Information System (ESDIS) project on 14 August 2017. (b) Vertical cross-
 1126 section along satellite's route (red line in c) of total attenuated backscatter at a wavelength of
 1127 532 nm obtained from the CALIOP lidar on 14 August 2017 at 6 UTC (black line denotes the
 1128 orography of the area). (c) Column-integrated BC concentration simulated with FLEXPART
 1129 (red line shows the path of the satellite). (d) Vertical distribution of BC concentrations with
 1130 longitude as seen with FLEXPART (grey area denotes the orography of the area).

1131



1132

1133 **Figure 7.** The instantaneous direct BOA RF due to (a) BC only, (b) BC and BrC, and (c) BC
 1134 and BrC when OC was assumed to be all BrC (extreme case) from the Greenland fire for
 1135 cloudy conditions on 31 August, 2017. (d) Daily variation of the TOA IRF over Greenland in
 1136 August 2017 for the three studied scenarios. Albedo reduction at 550 nm due to (e) BC only,
 1137 (f) BC and BrC, and (g) BC and BrC when OC was assumed to be all BrC (extreme case).
 1138 Note that the maximum albedo change due to deposited smoke is 0.00585 (BC only), 0.00590
 1139 (BC+BrC) and 0.00670 (BC+BrC extreme).

1140 **SUPPLEMENTARY FIGURE LEGENDS**

1141

1142 **Figure S 1.** Annual number of active fires over Greenland during the last 17 years as seen
1143 from NASA's MODIS satellite (product MSC14DL).

1144

1145 **Figure S 2.** Fire dynamics in Greenland for the August 2017 fires according to MODIS
1146 (magenta dots show active fire hot spots from the MODIS MCD14DL product). Locations of
1147 stations with AOD measurements from AERONET are also shown.

1148

1149 **Figure S 3.** Median injection heights (km above sea level – ASL; left panel) and distribution
1150 of longitudinally integrated burned biomass (Tg) as a function of injection altitude (right
1151 panel) calculated by PRMv2 for the period between 31 July and 21 August 2017.

1152 **Figure S 4.** Dry to total deposition ratio (example for BC) from the 2017 peat fires over
1153 Greenland.

1154

1155 **Figure S 5.** Relative standard deviation of deposited mass (example for BC) for different
1156 assumed size distributions normalized against the results from our reference size distribution
1157 with a logarithmic mean diameter of 0.25 μm . Particle size distributions with aerodynamic
1158 mean diameters of 0.1, 0.25, 0.5, 1, 2, 4, 8 μm and a logarithmic standard deviation of 0.3
1159 were simulated.

1160

1161 **Figure S 6.** Footprint emissions sensitivities for Northwestern, Northeastern, Southwestern
1162 and Southeastern Greenland for the period 31 July to 31 August 2017. Active fires from
1163 NASA's MODIS MCD14DL product are shown with red dots.

1164

1165 **Figure S 7.** Average contribution of biomass burning (upper panels) and anthropogenic
1166 emissions (lower panels) to surface concentrations of (a) BC and (b) OC in Northwestern,
1167 Northeastern, Southwestern and Southeastern Greenland (in ng m^{-3} per grid cell). Numbers (in
1168 red) represent total concentrations in the studied domain, obtained by spatial integration over
1169 all source grid cells. Receptor areas in Greenland are highlighted by pink boxes.

1170

1171 **Figure S 8.** (a) The single scattering albedo (SSA) of BC as a function of wavelength for
1172 various modified combustion efficiencies (MCE). The star and dot marked lines are from the
1173 parameterization of Pokhrel et al. (2016). (b) The IRF as a function of BC deposited on the
1174 Ice Sheet. The calculations were made for cloudless conditions with a snow-covered surface
1175 for noon on 31 August 2017 at 65°N.

Table 1. Start and end date of releases, source of data, type of sensor, burned area and daily increment of burned area, fuel consumption and calculated BC emissions from Eq. 1 during the Greenland fires in 2017. Total numbers for burned area, fuel consumption and BC emissions are highlighted in bold.

Start	End	Source of RS data	Type of sensor	Burned area (ha)	Increment of burned area (ha)	Fuel consumption (t C)	BC emissions (kg)	OC emissions (kg)	BrC emissions (kg)
31/07/17	02/08/17	Sentinel 2A	MSI	304	304	15176	3035	94543	18211
02/08/17	03/08/17	Landsat 8 OLI	MSI	428	125	6247	1249	38916	7496
03/08/17	04/08/17	Sentinel 1A	SAR	588	160	7980	1596	49712	9575
04/08/17	05/08/17	Sentinel 1A	SAR	740	152	7621	1524	47479	9145
05/08/17	07/08/17	Sentinel 2A	MSI	1100	359	17966	3593	111925	21559
07/08/17	08/08/17	Sentinel 2A	MSI	1314	214	10706	2141	66698	12847
08/08/17	12/08/17	Landsat 8 OLI	MSI	1868	554	27714	5543	172658	33257
12/08/17	14/08/17	Sentinel 1A	SAR	2005	136	6817	1363	42470	8180
14/08/17	15/08/17	Sentinel 1A	SAR	2169	165	8244	1649	51363	9893
15/08/17	16/08/17	Sentinel 1A	SAR	2209	40	1998	400	12444	2397
16/08/17	19/08/17	Sentinel 1A	SAR	2254	44	2213	443	13784	2655
19/08/17	21/08/17	Sentinel 2A	MSI	2345	92	4579	916	28530	5495
TOTAL					2345	117259	23452	730524	140711

RS - Remote Sensing

MSI - Multispectral Images

SAR - Synthetic Aperture RADAR

